nagra.

Arbeitsbericht NAB 13-88

Local stress field sensitivity analysis - Case Study Nördlich Lägern

August 2014

O. Heidbach, T. Hergert, K. Reiter, S. Giger

**Nationale Genossenschaft
für die Lagerung
radioaktiver Abfälle**

Hardstrasse 73
CH-5430 Wettingen
Telefon 056-437 11 11

www.nagra.ch

nagra.

Arbeitsbericht NAB 13-88

Local stress field sensitivity analysis - Case Study Nördlich Lägern

August 2014

O. Heidbach, T. Hergert, K. Reiter, S. Giger

KEYWORDS
Geomechanics, stress modelling, Finite Element Modelling, Spannungen, Nördlich Lägern

**Nationale Genossenschaft
für die Lagerung
radioaktiver Abfälle**

Hardstrasse 73
CH-5430 Wettingen
Telefon 056-437 11 11

www.nagra.ch

Nagra Working Reports concern work in progress that may have had limited review. They are intended to provide rapid dissemination of information.

Summary

For the region of Nördlich Lägern an existing geological model of the subsurface, consisting of lithological interfaces and faults is used as a basis for a geomechanical numerical model to conduct a sensitivity study of the 3D in situ stress state. Due to uncertainties regarding geometries and rock properties in the subsurface, the model exhibits generic features. Accordingly, the focus of the model is not on the precise quantification of the stress state, but on the estimation of the impact of individual factors contributing to the stress state and its spatial variability.

Based on the chosen modelling approach the results indicate that the relevant stress ratios S_H/S_V, S_h/S_V and S_H/S_h are considerably reduced in the Opalinus Clay in comparison to the formations lying above or below. Apart from local exceptions the stress conditions in the Opalinus Clay are only moderately affected by the parameter variations considered in the modelling runs and typically result in stress ratio values of $1.1 < S_H/S_V < 1.3$, $0.8 < S_h/S_V < 1.0$ and $1.2 < S_H/S_h < 1.4$. The stiffer formations, characterized by higher stress ratios and higher differential stress than the softer formations, show a more compressive stress regime and greater horizontal stress anisotropy and thereby support the push from the far field. The E-W striking faults reduce this push by thrust faulting, but also by lateral displacements enabling extrusion. Variation of stiffness by 33% in the formations directly above (Upper Dogger) or below (Lias and Upper Mittelkeuper) the Opalinus Clay results in a decrease of S_H/S_h by 0.1.

Of greater importance is the coefficient of friction on the faults. Higher fault friction increases stress ratios in the host rock, particularly horizontal stress anisotropy is increased (S_H/S_h increases by 0.1-0.2 when increasing the friction coefficient from 0.2 to 0.6) because the fault's ability to slip and thereby weakening the push from the far field is reduced at higher friction. Incorporation of a generic back-thrust adjacent to the Siglistorf anticline reduces stress ratios in the surroundings. However, at the depth of the Opalinus Clay its influence is only minor. Whether faults reach below the Mesozoic sediments or not does not much alter the stress state within the sediments. If a detachment horizon is present, stress ratios are strongly reduced north of the E-W striking faults.

Topography influences the stress state due to the spatially varying weight acting on the subsurface. However, of greater importance are those stresses that are induced by the topography as a response to the northward directed push from the far field. These induced stresses are positive below topographic depressions and negative below topographical highs and appear to depths of up to several hundred metres. An ice cover significantly lowers stress ratios and their lateral variability, particularly the ratio of horizontal to vertical stress is reduced.

Zusammenfassung

Für das Gebiet um Nördlich Lägern wurde ein bestehendes geologisches Modell des Untergrunds, bestehend aus Schichtgrenzen und Störungen als Grundlage für ein geomechanisches numerisches Modell verwendet, um die Sensitivität des 3D in situ Spannungszustands zu untersuchen. Aufgrund von Unsicherheiten hinsichtlich der Geometrien und Gesteinsparameter im Untergrund weist das vorgestellte Modell generische Züge auf. Entsprechend liegt der Schwerpunkt des Modells nicht auf einer präzisen Quantifizierung des Spannungszustands als vielmehr auf der Abschätzung des Einflusses einzelner Faktoren auf den Spannungszustand und auf dessen räumliche Variabilität.

Unter den gemachten Annahmen zeigen die Modellergebnisse, dass die relevanten Spannungsverhältnisse S_H/S_V, S_h/S_V und S_H/S_h im Opalinuston deutlich erniedrigt sind im Vergleich zu den meisten anderen Gesteinsschichten. Von lokalen Abweichungen abgesehen sind die Spannungsverhältnisse im Opalinuston für die betrachteten Parameterstudien relativ konstant und betragen $1{,}1 < S_H/S_V < 1{,}3$, $0{,}8 < S_h/S_V < 1{,}0$ und $1{,}2 < S_H/S_h < 1{,}4$. Die steiferen Formationen, die durch höhere Spannungsverhältnisse und Differenzspannungen charakterisiert sind als die weicheren Formationen, weisen ein kompressiveres Spannungsregime und größere transversale Spannungsanisotropie auf und tragen somit den Schub aus dem Fernfeld. Die O-W streichenden Störungen erniedrigen diesen Fernschub durch Überschiebung, aber auch durch laterale Verschiebungen, die Extrusion bewirken.

Eine Variation der Steifigkeit um 33% in den Formationen direkt oberhalb (Oberer Dogger) und unterhalb (Lias und Oberer Mittelkeuper) des Opalinustons führt zu einer Verringerung von S_H/S_h um 0,1. Von grösserer Bedeutung ist der Reibungskoeffizient auf den Störungen. Höhere Reibung erhöht die Spannungsverhältnisse im Wirtsgestein; insbesondere die horizontale Spannungsanisotropie erhöht sich (S_H/S_h erhöht sich um 0,1-0,2, wenn der Reibungskoeffizient von 0,2 auf 0,6 erhöht wird), weil das Vermögen der Störung, Versatz aufzunehmen und dadurch den Fernschub zu schwächen, reduziert ist. Das Einbringen einer generischen Rücküberschiebung neben der Siglistorf Antiklinale, verringert die Spannungsverhältnisse in der Umgebung, aber der Einfluss in der Tiefe des Opalinustons nur gering. Ob sich die Störungen unterhalb der Mesozoischen Sedimente fortsetzen oder nicht, ändert den Spannungszustand innerhalb der Sedimente nur unwesentlich. Falls ein Abscherhorizont vorhanden ist, sind die Spannungsverhältnisse nördlich der O-W streichenden Störungen stark reduziert.

Die Topographie beeinflusst den Spannungszustand aufgrund des lateral veränderlichen Gewichts, das auf den Untergrund wirkt. Von grösserer Bedeutung sind jedoch Spannungen, die durch die Topographie induziert werden als Antwort auf den nordwärts gerichteten Fernschub. Diese induzierten Spannungen sind positiv unter topographischen Senken und negativ unter topographischen Erhöhungen und erscheinen bis in Tiefen von mehreren hundert Metern. Eine Eisdecke erniedrigt die Spannungsverhältnisse deutlich, sowie ihre laterale Variabilität, insbesondere das Verhältnis von horizontaler zu vertikaler Spannung ist erniedrigt.

Table of Contents

List of Tables

List of Figures

1 Introduction

1.1 Motivation and in situ stress data

As part of the Sectoral Plan Deep Geological Repositories, all stress data for Switzerland and adjacent regions from the World Stress Map database release 2008 were re-assessed and new data records were added (Heidbach & Reinecker, 2013). In total the dataset for Switzerland and adjacent regions has now 567 data records with 289 of them with reliable A-C quality (Heidbach & Reinecker, 2013). The overall stress pattern of Northern Switzerland shows a long wave-length trend with a mean orientation of the maximum horizontal stress S_H of 160 ± 21° (Fig. 1.1-1). Northeast of Lake Constance S_H is N-S oriented and rotates gradually counter-clockwise by 20-25° to northwest Switzerland. S_H is oriented perpendicular to the gradient of the Alps, the Moho and the basement and sub-parallel to the indentation direction of the Adriatic plate with Eurasia indicating that these large-scale density contrasts and the plate tectonic setting are the key control of the overall stress pattern in Northern Switzerland.

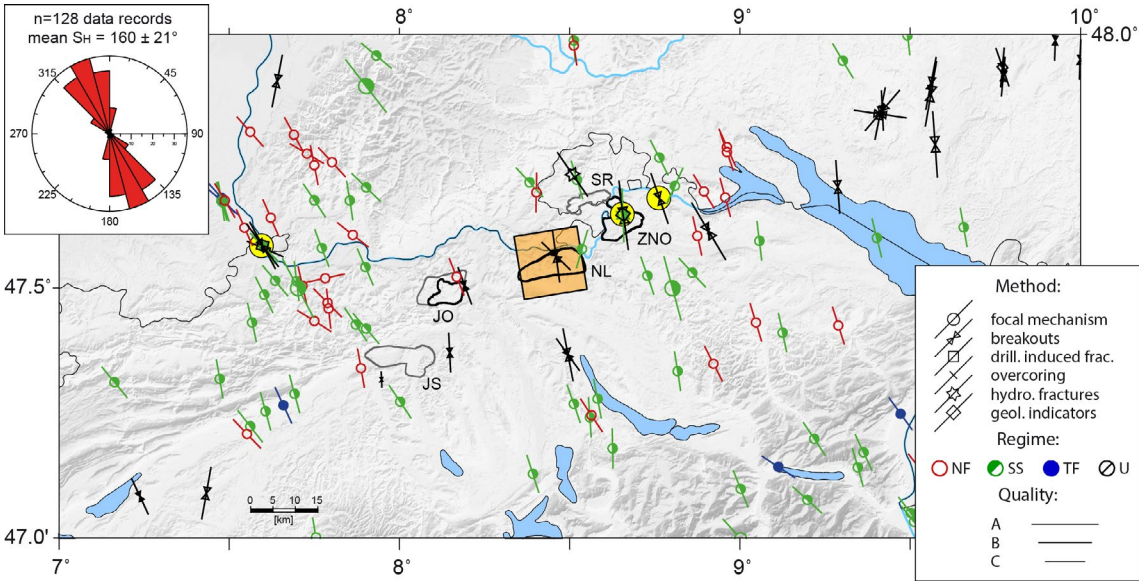

Fig. 1.1-1: Stress data in northern Switzerland and location of the model area.

Displayed are the A-C quality data records of the revised WSM database release 2008 (Heidbach et al., 2010; Heidbach & Reinecker, 2013). Bars indicate S_H orientations and symbols stress indicator. Colours indicate stress regimes with red for normal faulting (NF), green for strike-slip faulting (SS), blue for thrust faulting (TF), and black for unknown regime (U). Yellow circles show the three sites where stress magnitude data are available (Basel, Benken, Schlattingen), orange square marks the area of the geomechanical-numerical model. Black lines encircle the geological siting regions for high level waste Nördlich Lägern (NL), Zürich Nordost (ZNO) and Jura Ost (JO); grey lines encircle the geological siting regions for low level waste Jura-Südfuss (JS) and Südranden (SR).

Within the geological siting region Nördlich Lägern only three data records of the S_H orientation are available (Fig. 1.1-1). Two data records are from the Weiach borehole that show a 135 ± 25° S_H azimuth for the shallow layers between 408-558 m drilled depth above the Opalinus Clay and 172 ± 20° S_H azimuth for depths between 560-2248 m. The third data record is derived from a focal mechanism solution of the M_L 3.1 Eglisau earthquake that occurred on September 9th 1999 at 2 km depth (Deichmann, 2010). The tectonic regime of this event is strike-slip indicating that the vertical stress S_V is between S_H and the minimum horizontal stress S_h.

For the planning of safe underground engineering activities and the assessment of the long-term stability of nuclear waste disposal sites knowledge of all six components of the site specific stress tensor is desired. Thus, in order to estimate the spatially continuous 3D stress tensor in the geological siting region Nördlich Lägern, a 3D geomechanical-numerical model is set up. Due to uncertainties in the structure of the geological model and in particular the rock properties, as well as the scarce stress data, the model has a semi-generic character. Although the capability of the model to predict the true absolute in situ stress state is limited, the relative influence on various stress controlling factors can be studied in principal. Therefore, the model focusses on a parameter sensitivity study in order to estimate their relative impact on the in situ stress state.

1.2 Aim and key questions

The key goal of the geomechanical-numerical model is to estimate the variability of the 3D in situ stress in the geological siting region Nördlich Lägern (Cantons Zürich, Aargau) due to stiffness and strength contrasts of the lithological formations, pre-existing and potential faults as well as topography effects and the impact of a future ice cover.

Specific questions addressed by the model are:

1. What is the contribution of local topography and deep Quaternary sediment channels on local stress field variations and to which depth can they be traced?
2. What is the impact of the elastic and plastic rock properties?
3. To what extent affects the fault friction coefficient and its variation the stress pattern?
4. What is the impact of tectonic faults (Baden-Irchel-Herden lineament, Siglistorf anticline and a generic backthrust) on the in situ stress field?
5. How does an ice-cover affect in situ stress?

1.3 Stress term definitions and parts of the stress field

In geoscientific and rock engineering literature there is no strict agreement on stress term definitions. Thus, a brief description is given on how stress terms are used in this report. Beyond these definitions we point out that in this study compression is positive in contrast to engineering convention where compression has a negative sign.

Tab. 1.3-1: Definition of stress terms.

Due to the fact that there is no strict definition of stress terms in the literature (e.g. Engelder, 1992; Jaeger et al., 2007; Zang und Stephansson, 2010; Zoback, 2010), a brief definition of the stress terms used in this report is given.

Term	Symbol	Definition/Comment
in-situ stress state	-	Undisturbed natural stress state; also called virgin stress state. In particular the in situ stress is the sum of all natural stress contributions and natural processes that influence rock stress state at a given point.
disturbed in-situ stress state	-	Denotes that the in situ stress is disturbed due to man-made changes in the underground or loads on the surface such as impoundment, drilling, tunnelling, mining, fluid stimulation, reservoir depletion, re-injection of waste water to name a few.
principal stresses	σ_1, σ_2, σ_3	The symmetric stress tensor can always be transformed into a principal axes system (Jaeger et al., 2007). The three remaining non-zero components in the diagonal of the matrix are the principal stresses where σ_1 is the largest and σ_3 the smallest ($\sigma_1 \geq \sigma_2 \geq \sigma_3$).

Term	Symbol	Definition/Comment
differential stress	$\sigma_d=\sigma_1-\sigma_3$	Difference between the largest and the smallest principal stress.
effective stresses	σ'	Effective stresses σ' are total stresses σ minus pore fluid pressure p_f.
vertical stress	S_V	The magnitude of S_v is the integral of the overburden. Only at the Earth surface S_V is one of the principal stresses; at greater depth S_V can deviate from a principal stress orientation.
Orientation of the maximum and minimum horizontal stress	S_H, S_h	Assuming that the vertical stress S_v is a principal stress at depth S_H und S_h are the other two principal stresses of the stress tensor. Otherwise S_H and S_h are the projections of the principal stresses into the horizontal plane.
stress regime	-	Relates to stresses: The stress regime is an expression of the relative magnitudes of the principal stresses. It can be expressed as a continuous value using the Regime Stress Ratio (RSR) with values between 0 and 3 (Simpson, 1997).
stress pattern	-	Spatial uniformity or variability of a certain aspect of the stress tensor e.g. the pattern of the S_H orientation (Heidbach et al., 2010; Zoback, 1992)
transient stresses	-	The far-field forces due to plate tectonics are constant over long distances (> 1000 km) and long-time scales (> 100 ka). However, close to active tectonics the stress state is perturbed locally within the seismic cycle and thus changes constantly. Also in areas with low viscosity or overpressured fluids close to lithostatic pressure the stress state can be transient due to short relaxation times or creep processes.
tectonic stresses	-	According to Engelder (1992) tectonic stresses are the horizontal components of the in situ stress state that deviate from a given reference stress state (e.g. uniaxial, lithostatic). In particular a reference stress state implies that $S_H=S_h$. However, definitions in the literature are not consistent. Tectonic stress must not necessarily equal the deviatoric stress which is the non-isotropic part of the stress tensor (the isotropic part is the mean stress σ_m or one third of the trace of the of stress tensor $\sigma_m = 1/3(\sigma_{11}+\sigma_{22}+\sigma_{33}) = 1/3(\sigma_1+\sigma_2+\sigma_3)$. This is only true when one assumes that the reference stress state is lithostatic ($S_H=S_h=S_v$ with the assumption that S_V is a principal stress).
remnant/ residual stresses	-	Due to high viscosity of the upper crust the response to any kind of load is mainly elastic with high relaxation times of tectonic stresses in the order of tens or hundreds of million years. Thus the stresses due to past geological processes can be stored over very long time spans and are called residual or remanent stresses (Friedmann, 1972; McGarr und Gay, 1978; Zang und Stephansson, 2010).
tectonic regime	-	Relates to fault kinematics: Thrust faulting, normal faulting and strike-slip after Anderson (1905). Only when faults are optimally oriented in the stress field the stress regime is coincident with the tectonic regime (Célérier, 1995; Hergert und Heidbach, 2011). Normal faulting: $S_v > S_H > S_h$; Thrust faulting: $S_H > S_h > S_v$; Strike-slip: $S_H > S_v > S_h$

The stress state in the Earth's crust is mainly controlled by the density distribution in the gravity field and by plate tectonics (Heidbach et al., 2010; Zoback, 1992). Heterogeneous and anisotropic properties of the rock material as well as active tectonics or inherited structures from past geological processes result in different responses to the far-field forces and thus result in regional to local perturbations of the stress field. In particular, stiffness and strength contrasts in sedimentary layers, detachment horizons and active faults can have a dominant contribution to the regional and local stress field variability (Heidbach et al., 2007). The far-field stresses with long wave-length (> 1000 km) are controlled by the movement of the tectonic plates and mantle convection (Heidbach et al., 2010; Richardson, 1992; Zoback et al., 1989) and can be considered as stationary over time-scales > 1 Ma (Bercovici et al., 2000). Active faults are of regional importance and lead to a temporal change of the stress field. The stresses imposed by the far-field are relaxed by deformation within the seismic cycle or by aseismic creep (Engelder, 1992; Heidbach et al., 2010; Heidbach et al., 2007; Zang und Stephansson, 2010; Zoback, 1992; Zoback et al., 1989).

Locally the stress field can also be altered due to man-made processes that can act on different time and spatial scales. The superposition of all natural processes and structures results in the in situ stress state (Fig. 1.1-3 and Tab. 1.3-2).

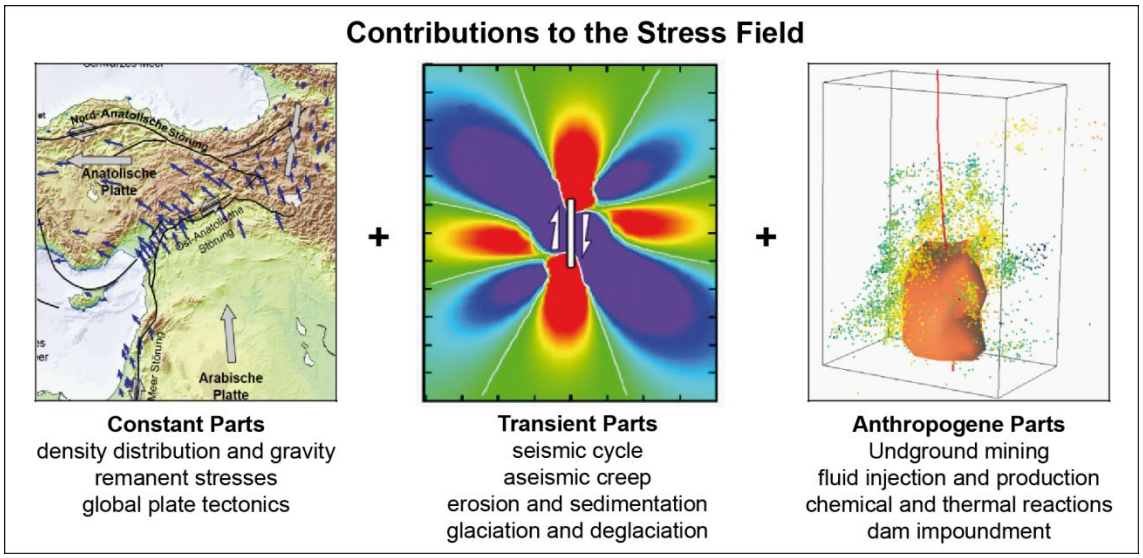

Fig. 1.3-1: Contributions to the stress field.
The contributions can be divided into three main parts that act on different temporal and spatial scales (Heidbach & Reinecker, 2013).

From an engineering perspective also the local, man-made stress changes are of great importance. Due to the removal of rock material, or due to an additional load e.g. by means of a filled dam, the in situ stress state is changed instantaneously and is changed mainly in the near-field of the causative process. Depletion of geo-reservoirs, re-injection of waste water or fluid stimulation is also affecting the fluid pressure significantly, leading to time-dependent stress changes due to pore pressure diffusion (Altmann et al., 2010). Furthermore, the re-injection of cold water or extraction of hot water has a thermal effect on the rock mass and may induce substantial thermal stresses. The same holds for heat generation due to the storage of nuclear waste. However, the impact or criticality in terms of the long-term stability of a tunnel, cavern, borehole etc. of these man-made stress changes depends on the present 3D in situ stress state, on the strength of the rock mass and on the stress change over time.

From a modelling point of view the determination of the man-made stress changes in a forward model is easier than determination of the initial stress field conditions, as most of the parameters needed to describe the man-made processes are known (amount and location of mass removal or replacement, production rate etc.). Also, the strength of the rock material can be estimated in an acceptable range of uncertainties, provided that samples from pilot drillings are available. The real challenge is the determination of the in situ stress state and its spatial variability as it defines *a priori* the criticality of a given site, i.e. how close the in situ stress is from either reactivation of a given fault structure or failure of intact rock. However, the information on in situ stress is in general sparse, incomplete and limited to a small number of data records derived from different stress indicators (Heidbach et al., 2007). Amongst these, earthquake focal mechanism solutions and borehole data are the most common. Furthermore, our knowledge is often limited to the S_H orientation (e.g. from borehole breakout data or drilling-induced tensile fractures), the magnitude of the minimum horizontal stress S_h (e.g. from leak-off tests or hydro-frac experiments) and the magnitude of the vertical stress S_V from density logs. In particular S_h magnitude data are often very rare. A new compilation of S_H orientations in Switzerland is presented in Heidbach & Reinecker (2013); stress magnitude data in Northern Switzerland are only available from boreholes in Benken, Schlattingen and Basel.

Tab. 1.3-2: Overview of components of the stress field and their wave-length.

The relative importance of different components of in situ stress at a given point can be derived from the spatial scale the individual contributions are acting on. The numbers given here are given for the most common setting, but local deviations of these can occur in dependence of the tectonic setting.

Structure/process	**Example**	**Scale [km]**
Plate boundary forces	Continental collision, sea-floor spreading, ridge push, subduction	10^3-10^4
Body forces	Large scale density contrasts due to mountain chains, continental shelf, Moho, sedimentary basins, river deltas, isostacy	10^2-10^4
Bending stresses	Glaciation and de-glaciation; fore bulge at subduction zones	10^2-10^4
Strong earthquakes	Mainly at the plate boundaries, but also intra-plate large events	10-10^3
Detachment horizons	Evaporate layers, faults with very low dip angle, layers with overpressured fluids	10-10^2
Geological structures	Faults, fracture networks, diapirs	0.01-10^3
Thermal stresses	Magma intrusions, advection, fluid circulation	0.01-10

1.4 Tectonic setting

The geological siting region Nördlich Lägern (Cantons Zürich, Aargau) is located in the northern part of the Central Swiss Molasse Basin (Nagra, 2008). At the potential repository level, the Opalinus Clay is part of the Deformed Tabular Jura. Within the model extent, the Opalinus Clay is present at a depth of approximately 500 to 860 metres below the surface and has a thickness between 100 and 120 metres. Compressive fault structures exist in the sedimentary cover with the Siglistorf anticline in the North and the Baden-Irchel-Herden lineament in the south. Deep-rooting, SW-ENE striking faults are interpreted as boundary faults of the Permo-Carboniferous Trough below the compressive structures (Diebold et al., 1991)

.

2 Model setup

2.1 Model assumptions and technical procedure

Key goal of the model is to estimate the contemporary 3D in situ stress and its variability due to fault structures (real and hypothetical ones), lithological formations and a presumed ice cover in the geological siting region Nördlich Lägern. We assume that transient and man-made processes can be neglected and thus only the contributions from gravitational forces and tectonic stresses are considered. As acceleration can also be neglected, we have to solve the partial differential equation of the equilibrium of forces. With a given elasto-plastic stress-strain relation this is a partial differential equation of second order with displacement u as the field variable.

To model the stress field two different approaches can be used: (1) Starting with first principles and simulate all relevant geological processes that caused the contemporary stress field, such as the collision of the Adriatic plate with Eurasia causing the growth of the Alps as well as the development of the Molasse Basin and subsequent northward shift of the sediments. This also would imply to consider the processes of erosion, sedimentation, compaction, glaciation and deglaciation. Even though scientifically interesting one would certainly not end with today's detailed 3D structure and the contemporary 3D in situ stress. (2) Starting with the contemporary geometry, i.e. fault structure, topography and lithological layers and parameterize the aforementioned tectonic processes in the area of interest by means of appropriate initial stress and kinematic boundary conditions (Henk, 2008; Hergert et al., 2011).

For the key questions to be addressed in this work we must follow the second approach. This leaves us with the problem to map all the past tectonic processes that contributed to the contemporary stress field into appropriate initial and kinematic boundary conditions. The initial stresses would equilibrate the gravitational stresses and resemble a reference stress state, whereas the kinematic boundary conditions are imposing the tectonic stresses. Furthermore, the choice of the model boundaries as well as the model dimension and orientation with respect to North, is of great importance when it comes to the definition of boundary conditions. The technical procedure we established for these kinds of models is explained in Fig. 2.1-1 with a schematic general workflow. The individual text boxes are color-coded indicating the four major steps in the course of the geomechanical-numerical model procedure.

In the first step (white boxes of Fig. 2.1-1) the model geometry is gathered and a 3D volume that consists of a number of sub volumes is generated. In particular the geometry includes the boundaries between mechanically significant layers, topography and the 3D major fault system. In a second step an appropriate initial stress state has to be defined that is in equilibrium with the gravity forces; the meaning of appropriate will be explained in a separate section later on. The kinematic boundary conditions are then used to impose the tectonic stresses from the geological history onto the model (grey boxes of Fig. 2.1-1). The third step is the model validation using model-independent observations (orange boxes in Fig. 2.1-1).

For the construction and discretization of the 3D model geometry we are using gOcad™ and HyperMesh™, respectively. For the solution of the resulting partial differential equation of the equilibrium of forces we are using the Finite Element Method (FEM) to solve an approximated solution numerically. The FEM is appropriate as is allows discretizing complex geometries with unstructured meshes. In particular the discretization of thin lithological layers, which is of key importance for this study, can be achieved. Furthermore, the commercial FEM software package Abaqus™ v6.11 has the capability to incorporate faults with Coulomb friction that can be reactivated. For the visualization we are using Tecplot 360™ extended with an own library that calculates from the resulting stress tensor a wide range of scalar values such as the Regime Stress Ratio (Simpson, 1997), magnitudes of S_H, S_h, S_V as well as ratios and orientations of these.

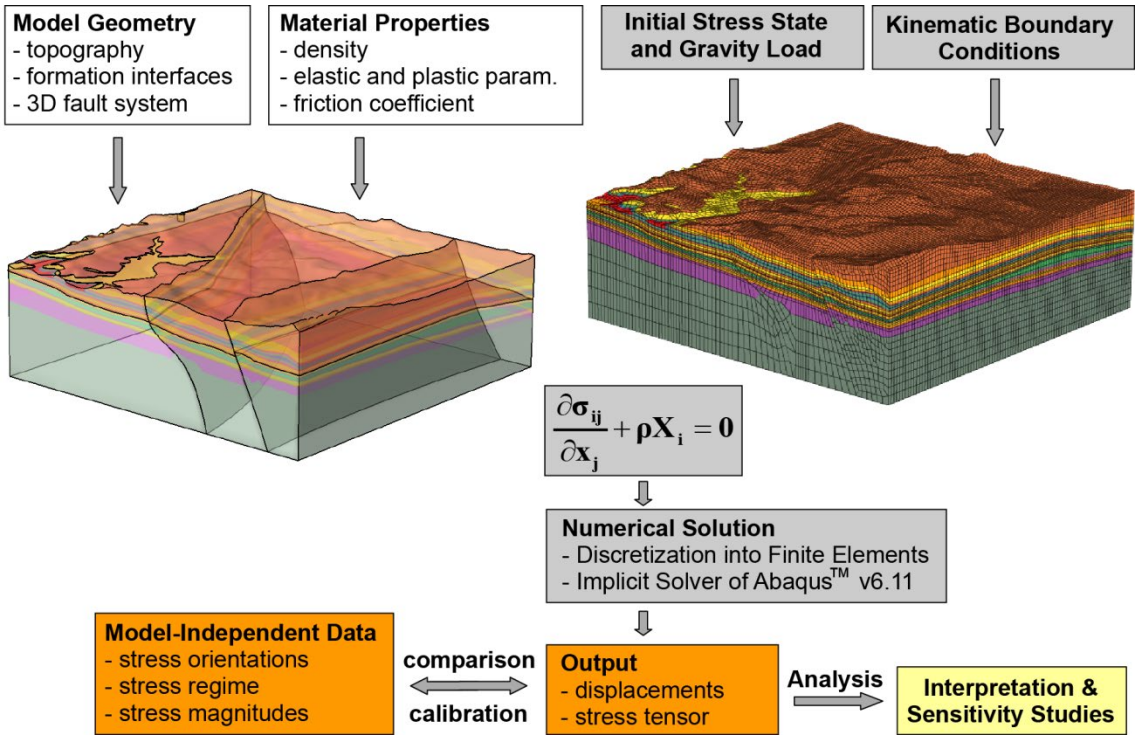

Fig. 2.1-1: General workflow of a 3D geomechanical-numerical modelling.

White boxes: Assembly of model geometry, rock properties and the 3D fault system. Left figure: 3D view of an arbitrary model structure. Grey boxes: Initial stress field and kinematic boundary conditions, loads and numerical solution. An appropriate initial stress state and kinematic boundary conditions are determined and applied as well as gravity and the load. Right figure: Discretised model volume. The partial differential equations of the equilibrium of forces in 3D are solved using the finite element method (σ_{ij} stress tensor, x_j Cartesian coordinates, ρ density, and X_i body forces). Orange boxes: Model results are calibrated against model-independent observations. Yellow box: Once the fit to the model-independent observations is acceptable, i.e. within their uncertainties, an interpretation and analysis of the model results can be performed. This should include a sensitivity analysis with respect to the uncertainties of the model parameters.

In the following sub-chapters we first describe in detail the construction of the model geometry and model boundary (2.2), its discretization (2.3), the used rock properties (2.4), the initial stress state calibration (2.5) and the kinematic boundary conditions (2.6).

2.2 Model geometry and boundaries

The geological local model NL is based on the geological 3D model of Switzerland which has been delivered by Nagra as a gOcad™ model (hereafter termed *outgoing model*). In this section the geometry of the geological model set-up is documented as well as the adjustments that were made to the outgoing model in order to perform the numerical stress-displacement analysis (*stress model*).

The outgoing model incorporates the Siglistorf anticline and the Baden-Irchel-Herdern (BIH) lineament as regional faults to the north and south of the siting region Nördlich Lägern, respectively. The stress model in its base case incorporates these two faults. Additionally, the stress model integrates a hypothetical back thrust fault, which forms a pop-up wedge with the Siglistorf anticline. Technically, the faults are represented as contact surfaces that allow relative dis-

placement once shear stress exceeds the strength of the fault which is defined by the coefficient of friction.

However, due to different requirements in terms of accuracy and sensitivity a number of corrections of the outgoing model had to be made. E.g. sharp edges within the horizons or intense curvature of the horizons, when approaching the intersections with the faults, do not affect the hydrogeological modelling, but would lead to artefacts in a geomechanical model. In the following three sub-sections we present first the implemented geological horizons and then explain in detail the changes made in the outgoing model regarding the faults and the horizons in particular in the vicinity of the faults.

2.2.1 Geological horizons

The geomechanical units (Fig. 2.2-1) were either directly taken as the geological units (e.g. Opalinus Clay) or were grouped (e.g. Upper Dogger) in order to avoid units with thickness less than 30-40 m. Contiguous sub formations of similar rheological rock properties within the Molasse and the respective Mesozoic formations have been grouped together as they become effective in the model only through their rock properties. Only the interface between the Upper Mittelkeuper and the Gipskeuper (i.e. top of Gipskeuper) was not directly taken from the outgoing model. The Gipskeuper in the interval Lias-Keuper is of geomechanical interest due to its elevated evaporate content. Therefore, a geomechanical unit Lias and Upper Mittelkeuper was introduced at the top of the Gipskeuper with a constant thickness of 64 m as in the Weiach wellbore (Fig. 2.2-1; Matter et al., 1988).

Stratigraphy		Thickness at borehole Weiach [m]	Geomechanical unit in the model
Quaternary		37	Quaternay cover (11)
Tertiary	OSM / OMM	-	Molasse (10)
	USM / Bohnerz Formation	149	
Malm	Felsenkalke to Villigen Formation	204	Upper Malm (9)
	Wildegg Formation (incl. Effingen Member)	87	Wildegg Formation (8)
Dogger	Wutach Formation to Murchisonae Oolith Formation	77	Upper Dogger (7)
	Opalinus Clay	112	Opalinus Clay (6)
Lias	Upper and Lower Lias	64	Lias and Upper Mittelkeuper (5)
Keuper	Upper Mittelkeuper		
	Gipskeuper (incl. Lettenkohle)	83	Gipskeuper (4)
Muschelkalk	Upper Muschelkalk	69	Upper Muschelkalk (3)
	Middle Muschelkalk	57	Middle and Lower Muschelkalk (2)
	Lower Muschelkalk	37	
Buntsandstein		10	
Paleozoic	Permo-Carboniferous / Crystalline Rocks		Pre-Mesozoic basement (1)

Fig. 2.2-1: Geological units of the model.

Simplification and arrangement of geological units into geomechanical model layers. The colour coding of the cells corresponds to the colour coding of the top layers of the formations in the profiles in Fig. 2.2-8 – Fig. 2.2.-13.

2.2.2 Corrections of the fault geometry

The geometry of the Siglistorf anticline in contact to the Pre-Mesozoic basement was modified to avoid small interior angles of the finite elements. The changed geometry of the fault in the critical section was set at minimum 25° between the fault and the top of the Pre-Mesozoic unit (Fig. 2.2-2). Furthermore, through this adjustment the ramp of the Siglistorf anticline in the outgoing model in the section between the interfaces top Pre-Mesozoic basement and top Middle and Lower Muschelkalk was eliminated (Fig. 2.2-2).

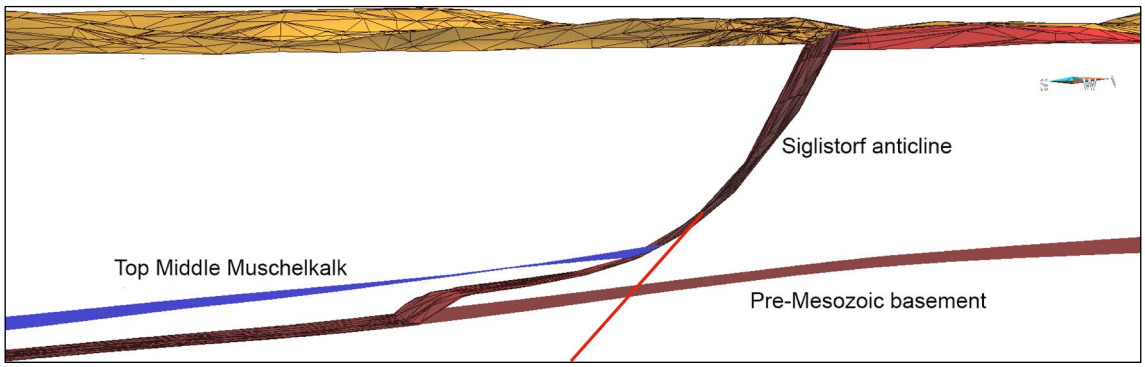

Fig. 2.2-2: Structure of the Siglistorf anticline.
The Siglistorf anticline was prolonged (red line) steeply dipping (at least 25°) into the Pre-Mesozoic basement unit to avoid small angles with the interfaces.

The complex structure of the BIH (Baden-Irchel-Herdern) lineament with a net normal faulting offset at the top Pre-Mesozoic basement and a net thrust faulting offset (Stadel-Irchel anticline) in the higher Mesozoic units was already simplified in the outgoing model by a single thrust (BIH) (Fig. 2.2-3) that extends well below the Mesozoic sediments (Fig. 2.2-3). The model geometry adopts this simplified BIH from the outgoing model although there is no evidence on the true depth extent of this structure below the Mesozoic sediments, and dip direction below the cover should merely be north instead of south (Fig. 2.2-3).

It was notified that in the outgoing model the simplified BIH lineament cuts the horizon top Pre-Mesozoic basement too far northerly in the western model area (Fig. 2.2-3 and Fig. 2.2-4). As a consequence, the horst of the normal faulting section of the BIH lineament is geometrically not represented in the simplification. Since the geological units had to be adjusted at the faults anyway (see sub-section 2.2.3) the interface top Pre-Mesozoic basement was adjusted at this location, while the BIH lineament was adopted without changes from the outgoing model in this respect. Furthermore, the BIH lineament in the outgoing model is undulating. The fault surface was smoothed, in particular in its deep part because its actual geometry is not well constrained by data there and it is likely that the undulation is simply an effect of the generation of a fault surface from profiles and thus an artefact. In the sediments the relocation is 10-40 m; at greater depth below the Mesozoic sediments the adaptation shift is > 100 m at some locations (Fig. 2.2-5).

Besides the Siglistorf anticline and the BIH lineament we include in the stress model a hypothetical antithetic back-thrust fault to the Siglistorf anticline. In particular, in the western part of the geological siting region there are indications for such a back-thrust on several NNW-SSE oriented seismic lines (see profile A in Fig. 2.2-3). The incorporated back-thrust only qualitatively represents these observations. It forms a wedge shaped block with the Siglistorf anticline (pop-up structure) and it is merely an artificial generic structure to investigate the influence of more complex fault zones. The back-thrust roots in the cutting line between the Siglistorf anticline and top Gipskeuper and dips uniformly at an angle of 50° to the north (Fig. 2.2-8-Fig. 2.2-13).

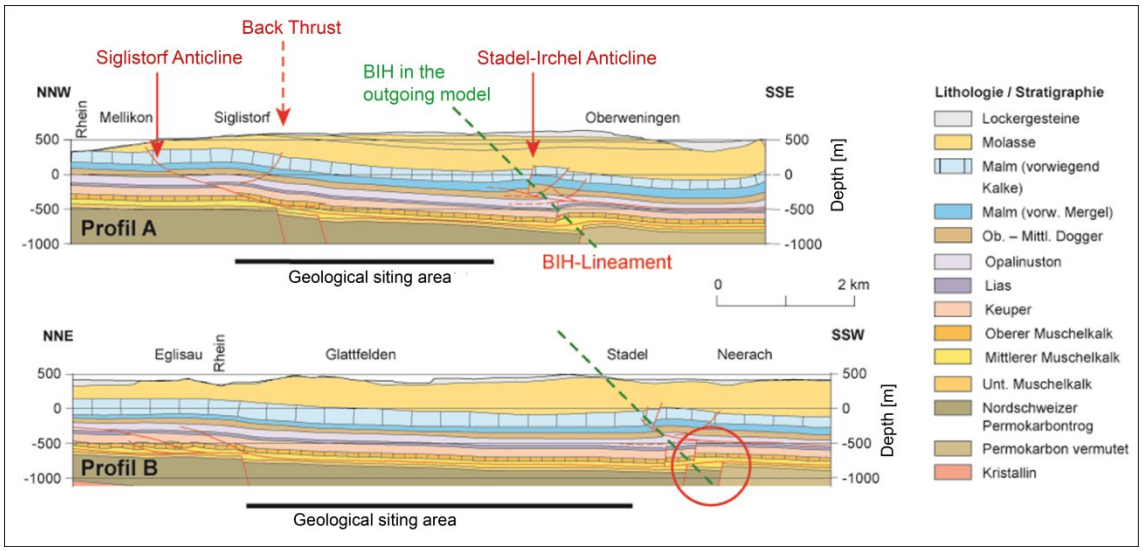

Fig. 2.2-3: Geological profiles through the model area.

The structural simplification of the complex interpreted fault pattern at the BIH lineament and the Stadel-Irchel-anticline by a single thrust fault in the outgoing model is shown schematically by the green dashed line. Red circle shows the discrepancy between the normal fault at top Pre-Mesozoic basement and the simplified fault geometry.

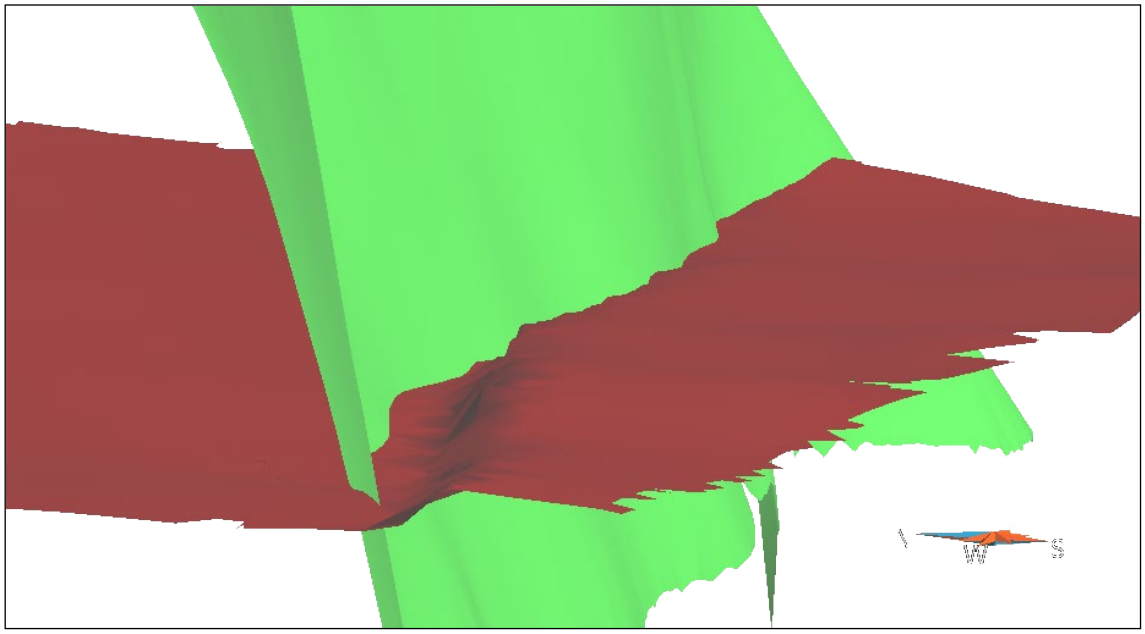

Fig. 2.2-4: Structure of the Baden-Irchel-Herden (BIH) lineament.

Geometrical relation between the BIH lineament as adopted from the outgoing model and the interface top Pre-Mesozoic basement (view direction ENE).

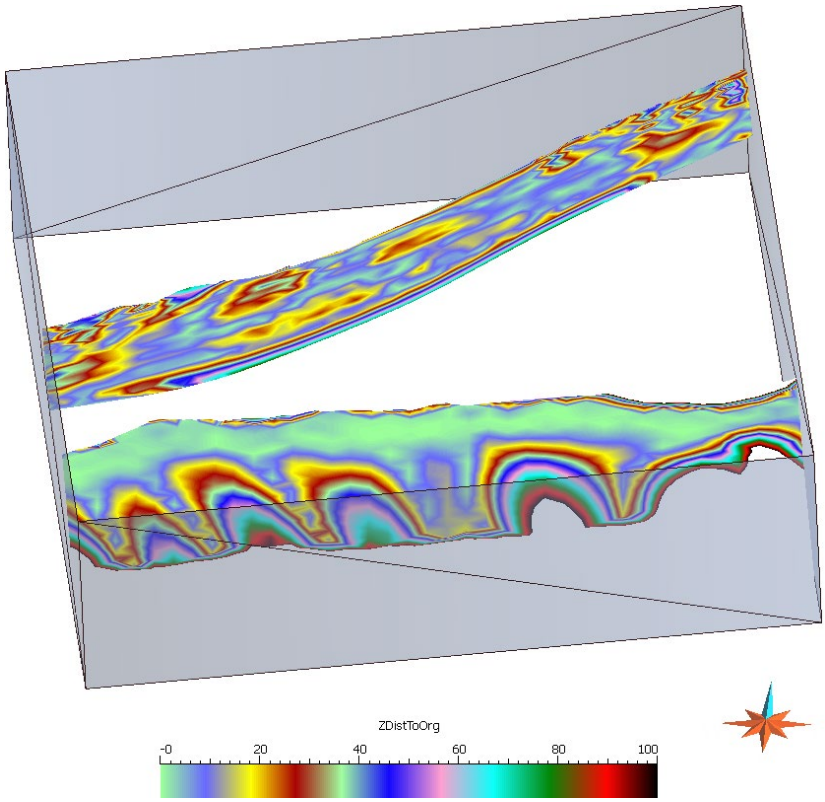

Fig. 2.2-5: Corrections of the fault structures.

Model box with the Siglistorf anticline (top) and the BIH lineament (below); view to north. Colours mark the distance between the original location in the outgoing model and new fault location in the stress model in meters. Note the regular smoothing of the probably artificial bends of the original BIH lineament.

2.2.3 Corrections of the horizon geometry

In the outgoing model certain features of the interfaces separating the geological formations were noticed, which obviously represent artefacts that appeared during construction of these interfaces (Fig. 2.2-6). These peaks were smoothed to avoid artefacts in the stress model results. This was done by extrapolating the horizons on the faults and trimming them with the fault surface. Furthermore, the geological horizons of the outgoing model are spatially continuous at faults even at vertical offsets. In order to prepare the geometry for the geomechanical model the horizons were also trimmed with the fault surfaces.

The result of the extrapolation and trimming as well as the deviation of the new interfaces from those of the outgoing model is shown along three profiles A-A' (Figs. 2.2-8 and Fig. 2.2-9), B-B' (Figs. 2.2-10 and Fig. 2.2-11) and C-C' (Figs. 2.2-12 and Fig. 2.2-13); the location of these profiles is shown in Fig. 2.2.-7. The horizons were prolonged to the south beyond the boundary of the outgoing model. The necessary changes were all in the order of a couple of tens of meters and thus have at most a local effect only.

At the postulated generic back-thrust in the model geometry, the geological interfaces of the respective formations are not vertically displaced relative to each other. This allows activation and complete removal of this fault as separate case studies.

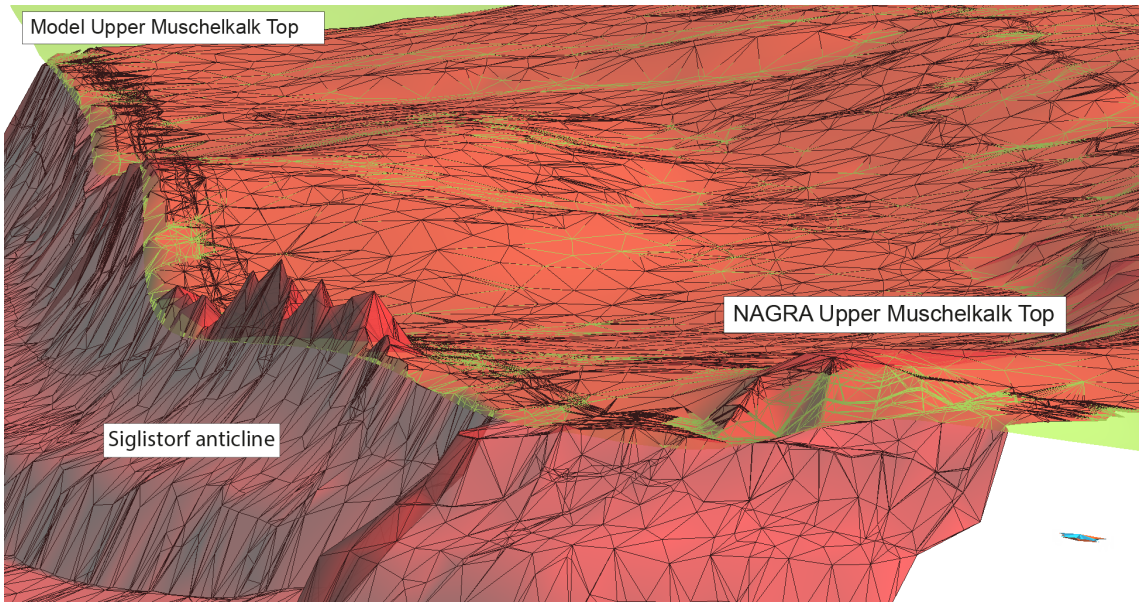

Fig. 2.2-6: Corrections of geometrical artefacts.
Artefacts of the interfaces in the vicinity of faults in the outgoing model (red) and the corrected surface (green).

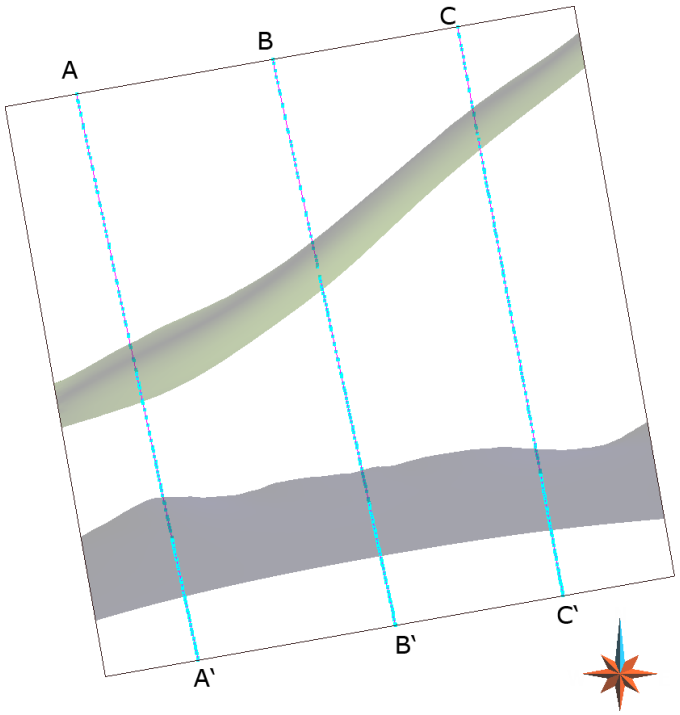

Fig. 2.2-7: Location of profiles through the geological model.
Overview of the model with location of the three profiles A-A‘ (Fig. 2.2-8 and Fig. 2.2-9), B-B' (Fig. 2.2-10 and Fig. 2.2-11) and C-C' (Fig. 2.2-12 and Fig. 2.2-13) relative to the Siglistorf anticline (north) and the BIH lineament (south).

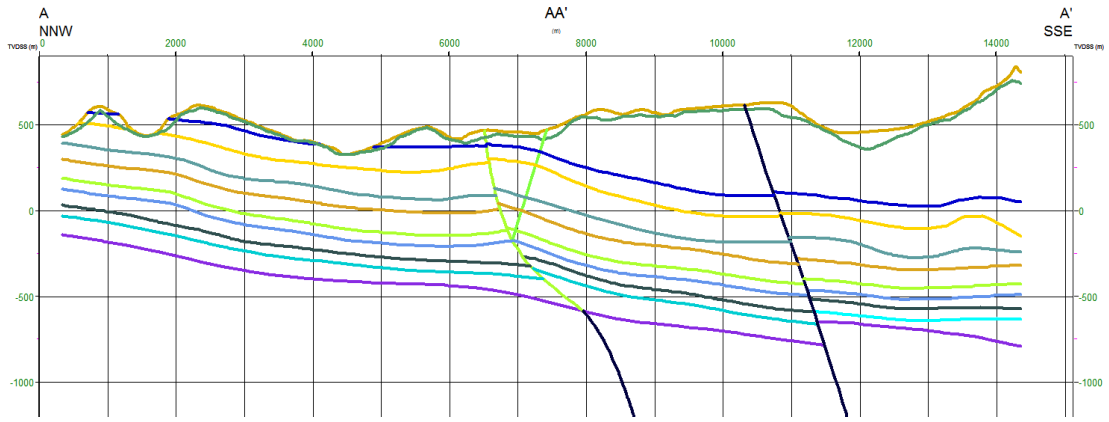

Fig. 2.2-8: Location of profile A-A’ through the geological model.
Profile A-A' of Fig. 2.2-7 with the new horizons (2.5 times vertically exaggerated). The colours of the lines refer to the tops of the formations in Fig. 2.2-1.

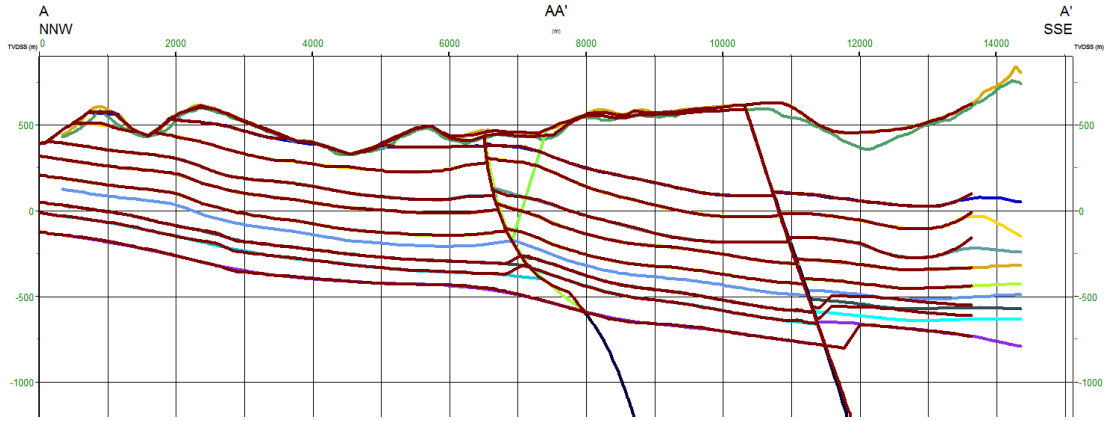

Fig. 2.2-9: New horizons of profile A-A’ through the geological model.
Profile A-A' of Fig. 2.2-7 with the new horizons (in colour in the background) and the horizons from the outgoing model (in dark red in the front), 2.5 times vertically exaggerated.

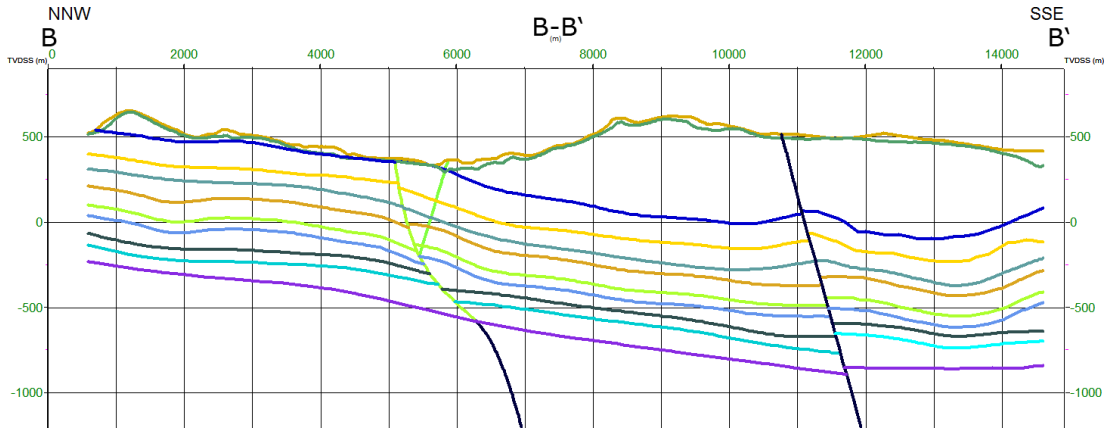

Fig. 2.2-10: Location of profile B-B’ through the geological model.
Profile B-B' of Fig. 2.2-7 with the new horizons (2.5 times vertically exaggerated). The line colours refer to the tops of the formations shown in Fig. 2.2-1.

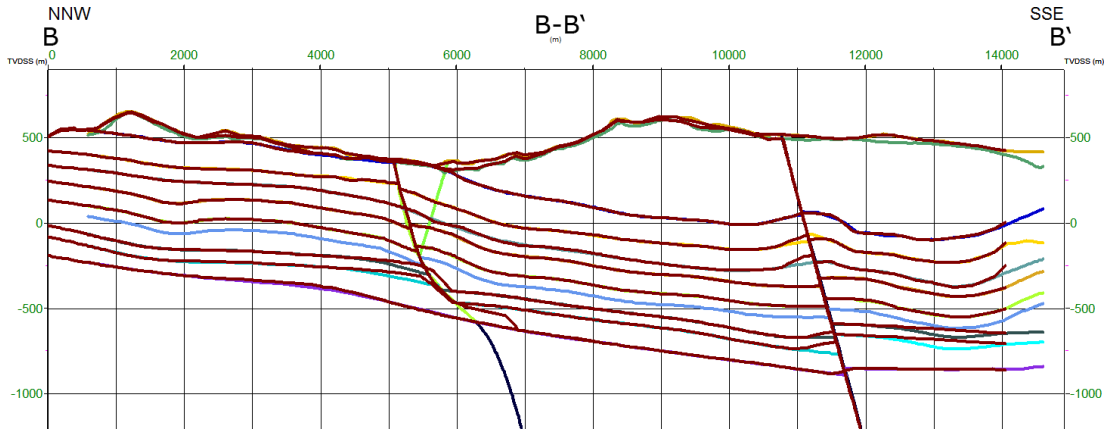

Fig. 2.2.-11: New horizons of profile B-B’ through the geological model.

Profile B-B' of Fig. 2.2-7 with the new horizons (in colour in the background) and the horizons from the outgoing model (in dark red in the front), 2.5 times vertically exaggerated.

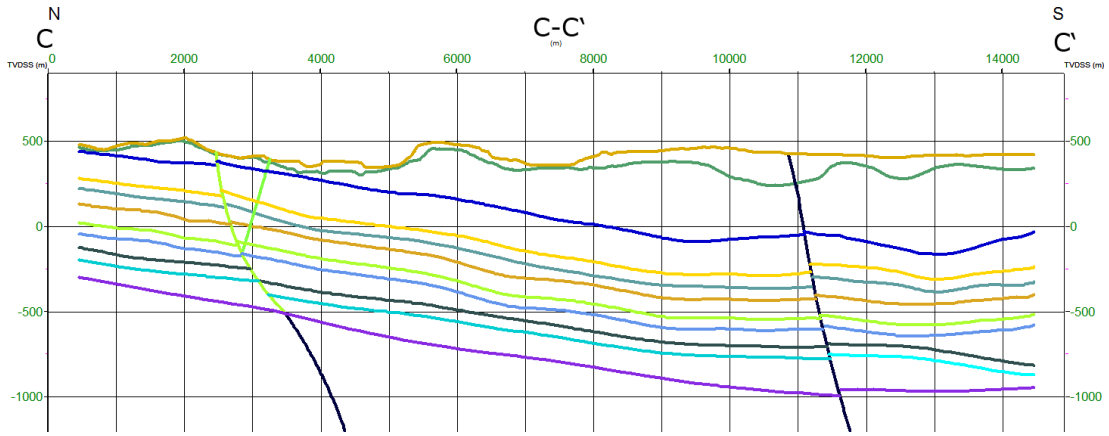

Fig. 2.2.-12: Location of profile C-C’ through the geological model.

Profile C-C' of Fig. 2.2-7 with the new horizons (2.5 times vertically exaggerated). The line colours refer to the tops of the formations shown in Fig. 2.2-1.

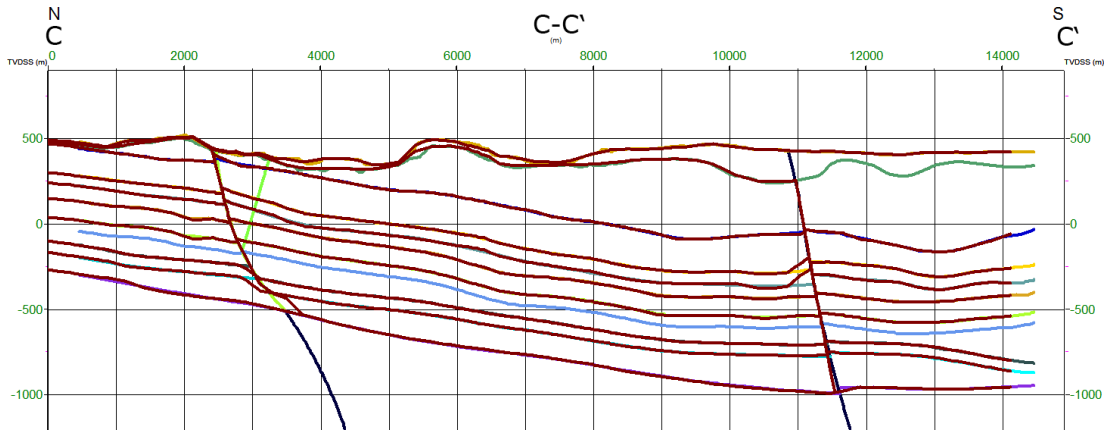

Fig. 2.2-13: New horizons of profile C-C’ through the geological model.

Profile C-C' of Fig. 2.2-7 with the new horizons (in colour in the background) and the interfaces from the outgoing model (in dark red in the front), 2.5 times vertically exaggerated.

During adjustment of the horizons at the Siglistorf anticline it was noticed that at a few locations (e.g. Top Wildegg Formation) the net offset in the outgoing model corresponds to a normal faulting displacement and not – as interpreted from the seismic lines – to a thrust faulting displacement. However, no changes in geometry were performed herein since a correction would be subjective to some degree. Furthermore, this inconsistency has an insignificant impact on the modelled stress field due to the very small and local density and stiffness contrast.

At some locations in the northern block of the model the thickness of formations is less than 15 m. These locations lie without exception close to the surface. Formations with small thickness (< 15 m) could have been only discretized with considerable additional effort and would increase computing time due to a substantial increase of the number of elements. The thickness of these formations was increased to 15-20 m at these locations. This increase in thickness is minor and close to the surface and its impact on the state of stress at the depth of the repository is negligible.

2.2.4 Model boundaries

The covered area of the model is quadratic with a side length of 14 km. The model boundary is rotated counter-clockwise by 10° with respect to a NS-EW orientation (Fig. 2.2-14). The bottom of the model is at 2500 m below sea level. The Siglistorf anticline and BIH lineament transect the model on its whole length from east to west and from the surface to the bottom of the model. This implies that these faults are effective in the model also below the Mesozoic formations although there is no clear evidence from geophysical data that these faults exist there. The following criteria were considered while determining the extent and arrangement of the model area:

- The geometric link between the SW-NE striking Siglistorf anticline and the SE-NW striking Mandach fault to the west is not clearly known. Thus, the western part of the tectonic structure is potentially not well represented in the model geometry.
- A sufficient wide extent of the model towards the south is required in order to allow the BIH lineament to be included in the model down to the bottom of the model. Therefore, the model reaches further to the south than the outgoing geological model. Accordingly, the interfaces of the lithological boundaries were extrapolated by 500 to 1000 m towards the southern border of the geomechanical model geometry.
- The northern boundary of the model corresponds to the erosive cut of the lithology in the Schwarzbach valley. This could not be fully avoided however the cut of all formations would considerably increase the efforts for discretization. Therefore, lithologies at the surface with a thickness less than 10 m were eliminated.
- The faults in the model area strike ENE, hence about 70-80°N. The revised interpretation of the S_H orientation in the Weiach wellbore states a S_H azimuth of 165-170°N (Heidbach & Reinecker, 2013). The model box was rotated counter clockwise by 10° which implies that the structures and stress data are oriented roughly parallel or perpendicular to the model boundaries, which facilitates the application of appropriate displacement boundary conditions.

The framework of regional faults (Albtal Graben southern border fault, Vorwald Fault, border faults of the North Swiss Permo-Carboniferous Trough) is not or only partially included in the local model NL, although the existence of the Hercynean faults (NW-SE striking) south of the Rhine is speculative. Therefore, the response of these regional faults to the far field stresses is not included in the local model NL.

In theory, the effect of structures outside the model area could be represented by appropriate kinematic boundary conditions. However, in practice this is difficult. At locations where faults

cut the model boundaries the relative displacement on faults would have to be defined at the model boundaries when using displacement boundary conditions and these would determine fault slip within the model area. Application of the sub-modelling technique would transfer the effect of structures outside of the local model area to its interior, but the regional faults are not included in the local model which would cause stress concentrations at the model boundaries.

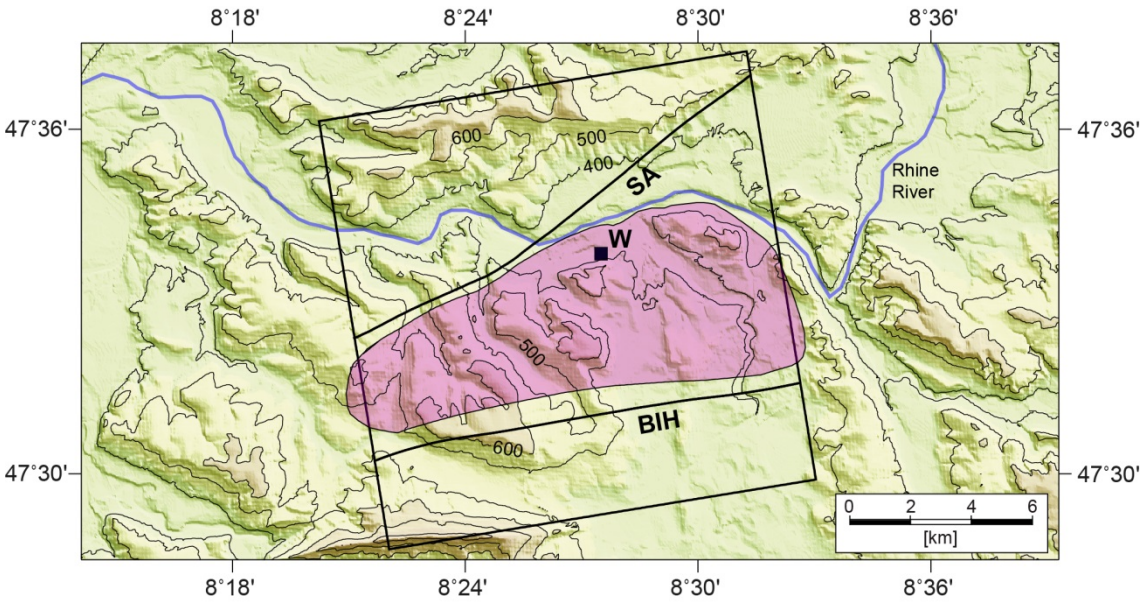

Fig. 2.2-14: Extent of the local model area Nördlich Lägern.

Black square shows model area (14 × 14 km^2). The BIH lineament and Siglistorf anticline (SA) cut through the whole model. Borehole Weiach (W) is indicated with the square and the geological siting region Nördlich Lägern is marked as the purple area. Topography contours are given in meters above sea level. Note variation of altitude c. 300 m within the model area.

2.3 Discretisation into finite elements

The geological model was discretized into 272,000 hexahedron elements with linear approximation functions (Fig. 2.3-1). Hexahedrons are less flexibly applicable than tetrahedron elements to describe complex 3D geometries, but they are numerically more precise than tetrahedron elements, having eight integration points instead of one for linear tetrahedron elements. Furthermore, hexahedron elements are practically the only possibility to represent thin layers of wide lateral extent as they are computationally stable for high aspect ratios of the lateral versus vertical element sides. With tetrahedron elements either the number of required elements would increase beyond feasible limits or the internal angles would run into critical values resulting in poor or no convergence after deformation of the model due to lateral kinematic boundary conditions.

Each of the Mesozoic formations is discretised by two layers of hexahedron elements, which corresponds to a vertical resolution between 15 and 130 m in the model area, mostly 30-50 m. The element size is similar in the overlying Molasse sediments. In the underlying Pre-Mesozoic basement the vertical resolution is lower. The lateral length of the element edges varies between 70 and 200 m. Fig. 2.3-2 gives the longest (left column) and shortest (right column) element edge as a measure for the spatial resolution.

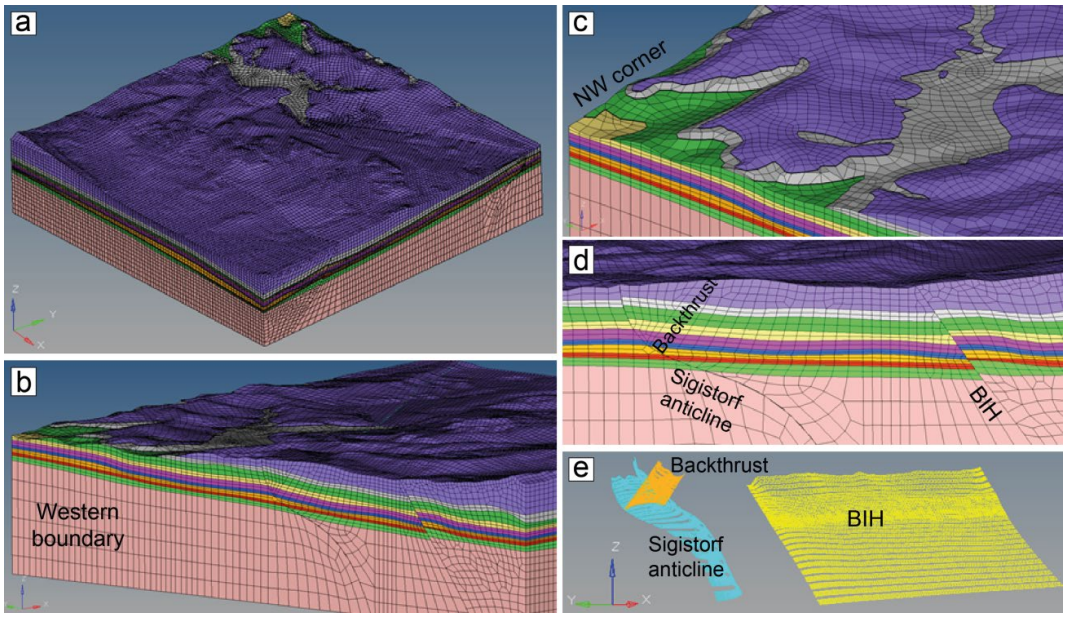

Fig. 2.3-1: Discretization of the model volume in finite elements.

a) View from SE to NW downward, b) Western model boundary, view to NE; Mesozoic formations become shallower from south to north, c) NW corner of the model, view to NE downward, Mesozoic formations cut the surface, d) western model boundary, view to W, cross section of the faults, e) only faults, view to NE. Formations are from top to bottom: Quaternary cover and Molasse, Upper Malm, Wildegg Formation, Upper Dogger, Opalinus Clay, Lias and Upper Mittelkeuper, Gipskeuper, Upper Muschelkalk, Middle and Lower Muschelkalk, Pre-Mesozoic basement.

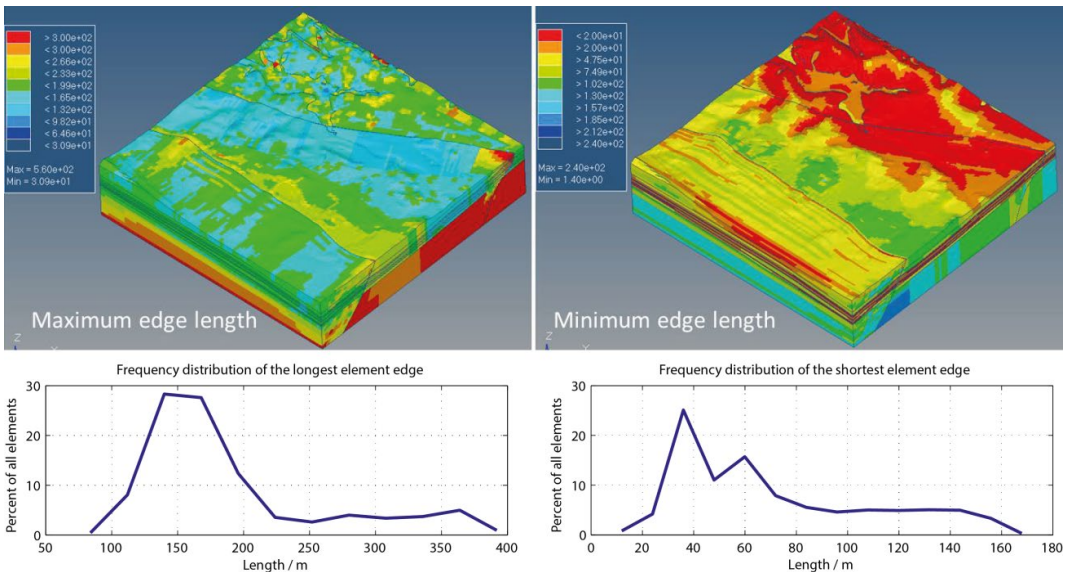

Fig. 2.3-2: Resolution of the model discretization.

Length of longest (left) and shortest (right) edge of the finite elements within the model area as contours (top) and as frequency distribution (bottom). This is a measure for the spatial resolution of the model. Left column mainly addresses horizontal resolution and right column the vertical resolution.

2.4 Rheological properties and density distribution

The physical rock properties of the individual formations considered in the model are summarized in Tab. 2.7-1. The listed properties in the orange columns are those of the base model and were provided by Nagra. Performed variations regarding the rock properties are documented in Section 2.7.

2.5 Stress state calibration

In a first step an initial stress state is established that is in equilibrium with gravity and ensures an appropriate ratio of horizontal to vertical stress. In a second step the kinematic boundary conditions are applied at the model boundaries to impose the horizontal far field tectonic stresses. In both steps separate calibrations are performed, for the initial stress state without tectonic stresses and for the final stress state with tectonic stresses.

2.5.1 Definition of initial stress

The initial stress state of the model considers no lateral tectonic loading and vertical and lateral stresses are controlled by gravity forces. In homogeneous, isotropic rocks, and assuming linear elastic behaviour and lateral kinematic constraints as a boundary condition, the horizontal stress (S_h) can be related to the vertical stress (S_v) through the Poisson's ratio (ν):

$$\frac{S_h}{S_v} = \frac{\upsilon}{1-\upsilon} \tag{1}$$

The geomechanical model is focussing on relatively shallow sediment layers. Equation (1) may be regarded as an appropriate first-order approximation for lateral stresses in rocks with low porosity (e.g. limestones, Pre-Mesozoic basement) or rocks with low clay mineral content (e.g. sandstones). For normally consolidated clays or clay-rich soils, the horizontal to vertical effective stress ratio (K') is generally approximated by $S_h'/S_V' \approx 1-\sin(\varphi)$ (Jáky, 1944), where φ is the effective friction angle. Empirical correlations have shown that the ratio of overconsolidated clays or shales during unloading (e.g. exhumation) are elevated with respect to values at identical depth during initial or normal loading (e.g. Brooker and Ireland, 1965). Mayne and Kulhawy (1982) suggested, the stress ratio relationship of normally consolidated clays be extended for overconsolidated clays or shales by taking into account the overconsolidation ratio (OCR), such that the effective stress ratio K' yields

$$K' = (1 - \sin\varphi) \cdot OCR^{\sin\varphi} \tag{2}$$

where OCR is the ratio of the maximum effective overburden stress experienced during its geologic history (S_{VC}') and the present effective overburden stress (S_V'). S_{VC}' can be estimated by oedometric testing (e.g. Ferrari et al., 2012) or a number of indirect methods (cf. Tables 3.3-1 and 3.3-3 in Nagra, 2002).

Applying Equation (2) to Opalinus Clay by using φ = 25° and OCR values from three sites in northern Switzerland, the depth-dependent effective stress ratio K' can then be approximated as

$$K' = 0.58 \cdot \left(1 + \frac{650}{z}\right)^{0.42} \quad . \tag{3}$$

where z is the present depth in metres. The resulting curve is given in Fig. 2.5-1 (left). Note that the green line represents a depth-trend of effective stress ratios for a situation without any lateral tectonic forces assuming validity of the semi-empirical approach formulated in equation (2).

Since the numerical modelling in this study is conducted using total stresses, the effective stress ratio K' has to be converted into total stress ratio K:

$$K = \frac{K'(S_V - P_P) + P_P}{S_V} \quad . \tag{4}$$

Assuming hydrostatic pore fluid pressure and a constant density of 2.5 g/cm^3, Equation (4) simplifies to:

$$K = 0.6 \cdot K' + 0.4 \quad . \tag{5}$$

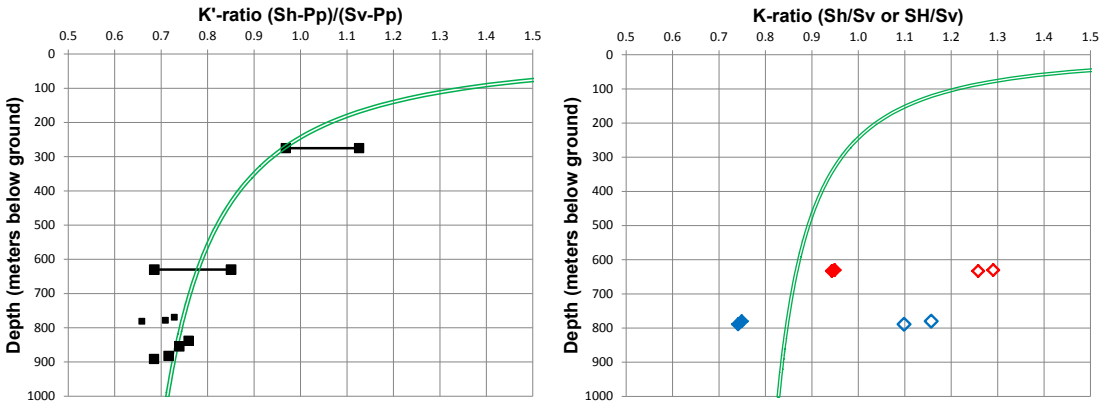

Fig. 2.5-1: Depth-dependent *effective* stress ratio of Opalinus Clay

Left: Effective stress ratio K' without tectonic loading. Black squares show calculated values for Opalinus Clay based on Equation (2), with overconsolidation ratios from the underground lab Mont Terri (present depth approximately 280 m, OCR≈4), and the boreholes Benken (~630 m, OCR≈2) and Schlattingen (~900 m, OCR≈1.7) and with φ=25°. The small squares represent data from Upper Dogger samples from Schlattingen with comparable clay mineral content as in Opalinus Clay. *Right:* Calculated total stress ratio K curve based on Equation (4) Depth-trend of total stress ratio used to calibrate the *initial* stress state for the Opalinus Clay in the model. The shown data points use hydraulic fracturing data and represent the in situ stress state including tectonic loading (blue=Schlattingen, red=Benken; filled diamonds = S_h/S_V, open diamonds = S_H/S_V). The stress ratios from hydraulic fracturing in Benken are used for calibration of the *final* stress in the model.

The resulting curve in Fig. 2.5-1 (right) represents the target total stress ratio K for the calibration of the initial stress state in the Opalinus Clay for the geomechanical-numerical model. Also indicated in the same figure are stress ratios estimated from hydraulic fracturing at the locations of Benken (Nagra, 2001) and Schlattingen (Klee, 2012) in Northeastern Switzerland. The hydraulic fracturing data represent the in-situ stresses, i.e. the stress state including tectonic loading. Conceptually, tectonic loading is interpreted for both S_h and S_H values at the Benken site when comparing to the green line, whereas slight tectonic unloading may be interpreted for the Schlattingen site. This is consistent with the tectonic setting as Schlattingen was drilled in the border zone of the Hegau-Bodensee Graben (Nagra, 2008).

2.5.2 Realisation of initial stress

Herein, calibration does not mean that the values for K are set as pre-defined values in the model at these points. Rather these values have to be attained independently in an equilibrated model volume experiencing gravity.

Technically, the initial state of stress was established by application of gravity on the model volume with its boundaries at the bottom and at the sides being fixed for displacements perpendicular to the model boundaries. The rock properties in the individual formations are given by Tab. 2.7-1 except the Poisson's ratios, which are ν=0.46 for the clay-mineral rich Opalinus Clay and Gipskeuper, ν=0.43 for the Pre-Mesozoic basement and ν=0.396 for all other formations. During uniaxial compaction the Poisson's ratio controls the horizontal stress and this mechanism is used to establish the stress state as defined in 2.5.1

Then the obtained stress state is implemented into an undeformed model with the real Poisson's ratios of the formations (and Young's moduli) as stated in Tab. 2.7-1 and three successive equilibration steps are performed in order to eliminate small residual displacements. In each of the equilibration steps the stress state resulting from the previous equilibrium step is used as starting stress for the next step. In the last step equilibrium displacements were smaller than a few centimetres. After the third equilibrium step it was tested whether the obtained stress state agrees with the initial stress state to be matched. Fig. 2.5-2 shows the modelled K-ratio in map view in the middle of the Opalinus Clay formation (left) and the difference between the modelled K-ratio and the theoretical K ratio from equation (5) (right). The K-ratio in the Opalinus Clay shows relatively small spatial variation between 0.8 and 0.95 in most of the model area, except near model boundaries, to the south of the Siglistorf anticline and in the north, where the Opalinus Clay comes close to the surface. The deviations with respect to the values of equation (5) are small except in the NW of the model area, where the Opalinus Clay is between 150-250 m below surface and thus strongly influenced by the prominent topography gradients in that area (Fig. 2.2-14). To the south of the Siglistorf anticline the K-ratio is obviously influenced by this fault so that there is no undisturbed, purely gravity-controlled stress state. In conclusion, the modelled stress state fits the theoretical one in areas not influenced by faults or topography and is therefore taken as initial stress state in the model.

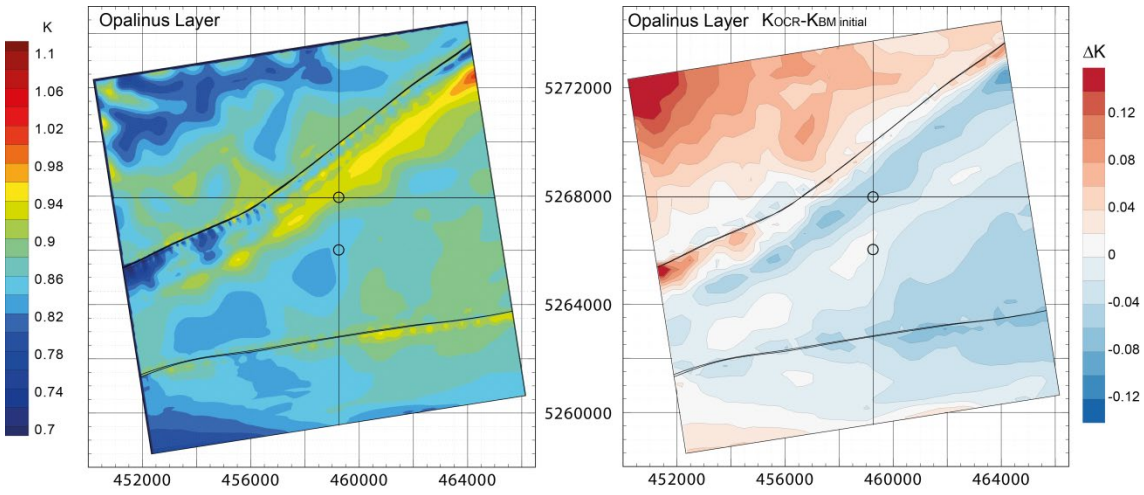

Fig. 2.5-2: S_h/S_V ratio from initial stress field of BM at the mean of Opalinus Clay formation.

Left figure shows K-ratios at the middle of the Opalinus Clay formation of the BM model without tectonic stresses. Right figure shows the difference between the theoretical K-ratio from the OCR curve in eq. (5) and the ones from BM initial. Thin lines are locations of profiles through the wellbore Weiach; small circles denote the location of the two depth profiles displayed in Fig. 2.5-3 the northern of which is the site of the Weiach borehole.

The initial stress state was also extracted at two vertical profiles from the model (Fig. 2.5-3). The K-ratio increases when approaching the surface. However, over the depth range of the model several jumps in K ratio appear which are due to the Poisson's ratios used in the compaction step. The clay bearing formations which had high Poisson's ratios in this step show greater K-ratios than the other formations which had a lower Poisson's ratio. The two profiles were taken at the location of the Weiach borehole and 2000 m south of it (Fig. 2.5-2). At the location of the Weiach borehole the middle of the Opalinus Clay is encountered at ~600 m depth and at that depth *K* should be 0.875 according to eq. (5). However, this site is in the surmised zone affected by the Siglistorf anticline and therefore does not perfectly match the theoretical value. However, the other location, 2000 m further south, is in between the Siglistorf anticline and the BIH and seems widely unaffected by these faults. Here, the Opalinus Clay is at ~800 m depth and *K* should be 0.845 from equation (5). At this site, good agreement is obtained between the modelled and theoretical K-ratio. For the different model variants considered (see Chapter 2.7) it was not tried to match the calibration data individually by modifying the Poisson's ratio during the first compaction step.

2.5.3 Final stress state

The initial stress in the model being established, displacement boundary conditions are applied at the lateral boundaries of the model to incorporate the tectonic stresses from the far field. Basically, the model is shortened in N-S direction and dilated in E-W direction (Chapter 2.6). To calibrate the final stress that includes tectonic stresses, we use the measured stress ratio $K = S_h/S_V = 0.94$ from hydraulic fracturing in the Opalinus Clay from the wellbore Benken (two closely spaced measurements only) (Nagra, 2001). Hence, it is assumed that stress at the Benken site is representative for the geological siting region of Nördlich Lägern some 10 km to the SW. The amount of displacement at the model boundaries was chosen such that the stress state in the Opalinus Clay in the model matches this value. Fig. 2.5-3 shows that $K \cong 0.95$ at 600 m depth at the Weiach borehole and $K \cong 0.934$ at 800 m depth at the location 2000 m south of Weiach.

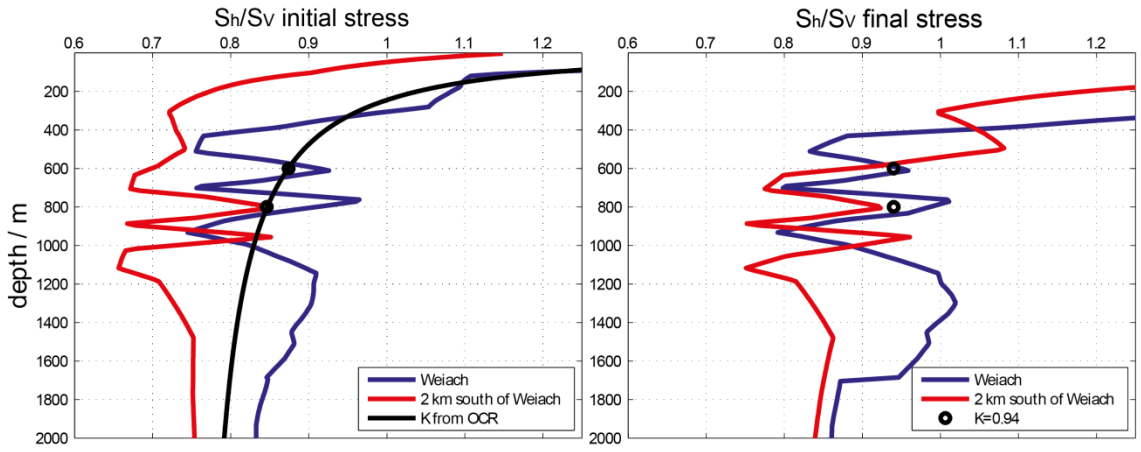

Fig. 2.5.-3: Depth profiles of S_h/S_V ratio of BM at Weiach and 2 km south of it.

Left figure shows the K-ratio from the initial stress field of BM. The black line corresponds to the green line in Fig. 2.5-1; right figure shows K-ratios from the BM with tectonic boundary conditions. Black circles on the right side are the K-ratios from Benken derived from hydraulic fracturing.

2.6 Boundary conditions

After the initial stress state is established and equilibrated with the gravity forces in the model, the tectonic boundary conditions are applied to incorporate the effect of the prevailing plate tectonic stress conditions of the geological past. The southern boundary of the model is displaced to the north by 9 m, perpendicular to the model boundary, while the boundaries in the west and east are pulled by 0.4 m each; the northern model boundary is fixed for displacements perpendicular to the boundary. Displacements parallel to the model boundaries are allowed everywhere. In the model variant that considers the decoupling horizon as frictional contact surface (GE) the push from south to north at the southern model boundary is applied only above the decoupling horizon, whereas below the decoupling horizon the southern model boundary is fixed for displacements perpendicular to the boundary. Displacements at the bottom of the model are constrained to zero in vertical direction while horizontal displacements are freely possible. The surface of the model is unconstrained.

The applied boundary conditions are very simple but try to integrate the available knowledge. Due to the slightly rotated boundaries of the model with respect to NS and EW the direction of the exerted push is perpendicular to the compressive structures in the sedimentary cover. The Jura main thrust, which is southwest of the area covered by the local model is oriented parallel to the southern model boundary (Fig. 2.2-14). Whether the S_H orientation in the basement is the same as in the sediments is not fully clear (Heidbach & Reinecker, 2013).

2.7 Overview of the model variants

The base model (BM) described in the previous sections was supplemented in several aspects in order to investigate the influence of different components of the model on the resulting stress field. Tab. 2.7-1 gives an overview of the performed model variants. The effective coefficient of friction on the faults of $\mu'=0.2$ in the base model was increased to $\mu'=0.6$ (model R06) and $\mu'=1.0$ (model R10) to study the effect of a higher degree of coupling of the involved blocks separated by the faults.

One model variant additionally includes the backthrust south of the Siglistorf anticline (model GR). As there is no clear evidence for the Siglistorf anticline and the BIH lineament penetrating the Pre-Mesozoic basement below the Mesozoic units, at least not in the way they were constructed, one model variant was tested in which both exist only above the Pre-Mesozoic basement (model GB). Due to technical reasons (the formations have vertical offsets across the Siglistorf anticline and BIH and therefore the mesh is discontinuous at the faults and cannot be equivalenced) these fault sections cannot be eliminated in the mesh. Instead, a very high coefficient of friction of $\mu'=100$ was assigned to the fault sections in the basement to represent strong coupling of the blocks in the basement. One model variant includes a frictional contact surface in the middle surface of the Middle Muschelkalk throughout the model area to simulate the effect of the proposed decoupling horizon (model GE). An alternative approach assumes plastic rheology in the bulk volume (models P1 and P2), where decoupling horizons may evolve independently. The Mohr-Coulomb criterion was applied. Values for friction angle and cohesion were provided by Nagra and are summarized in Tab. 2.7-1.

The model variant E0 assumes homogeneous distribution of rock properties throughout the model volume ($\rho=2.6$ g/cm³, $E=25$ GPa, $\nu=0.26$). This implies that the formations included in the model have no individual influence on the stress field except the surface topography. The purpose behind this model variant is that effects of topography and faults are no longer concealed by the effects of spatial variations of density and elastic parameters. Four further model variants assume increased or decreased stiffness by 33% in the formations above (Upper Dogger) and below (Lias and Upper Mittelkeuper) the Opalinus Clay (models E1-E4).

The influence of an ice sheet covering the model area is also investigated. Two model variants assume a flat surface of the ice sheet, which implies spatially variable thickness of the ice due to topography. Both a thin (ice surface at 500 m above sea level) (model I500) and a thick (ice surface 1000 m above sea level) (model I1000) ice sheet were tested. Further, the case of constant thickness (500 m) of the ice sheet is tested, which implies that the surface of the ice sheet has the same shape as the underlying topography (model I500s). In all cases the load exerted by the ice is applied after the tectonic boundary conditions are in effect.

Tab. 2.7-1: Description of the model variants.

BM=Base Model with values in orange fields. In the model variants only the changes with respect to BM are stated.

	BM			R06	R10	GR	GB	GE	E0	E1	E2	E3	E4	I500	I1000	I500s	P1/P2	
	ρ g/cm³	ν	E GPa							E GPa	E GPa	E GPa	E GPa				ϕ deg	C MPa
Molasse and Quatenary cover	2.35	0.29	15						ρ= 2.6 g/cm³ ν=0.26 E=25 GPa								38	10
Upper Malm	2.68	0.25	40														50	20
Wildegg Formation	2.65	0.29	15														40	8
Upper Dogger	2.55	0.27	15							20	20	10	10				30	8
Opalinus Clay	2.5	0.29	10														23	4
Lias and Upper Mittelkeuper	2.45	0.25	15							20	10	20	10				30	8
Gipskeuper	2.7	0.25	20														34	28
Upper Muschelkalk	2.65	0.25	40														45	23
Middle & Lower Muschelkalk	2.65	0.25	20														40	20
Pre-Mesozoic basement	2.6	0.25	30														40	30
μ'	0.2			0.6	1.0	0.2 for back thrust	0.2 in sediments, 100 in basement	Mid surface of Middle Muschelkalk active (μ'=0.2)									P1: μ'=0.2 P2: μ'=0.2	
Kinematic boundary conditions	9 m push South 0.4 m pull West & East 0 m North each perpendicular to boundary orienation							push only above mid surface of Middle-Lower Muschelkalk									P1: as BM P2: 30 m push 3 m pull	
Loads	Gravity													Ice coverage with ice surface @ 500m a.s.l.	Ice coverage with ice surface @ 1000m a.s.l.	Ice coverage with constant thickness of 500 m		

3 Results of the base model

The results of the base model BM are presented in terms of displacements and stresses on vertical cross sections in NS and EW direction through the Weiach borehole and as maps in the middle surface of the Opalinus Clay as well as at a constant depth of 300 m bsl.

3.1 Kinematic results of the base model

The Siglistorf anticline shows left-lateral offset that increases towards the surface, while the BIH lineament shows right-lateral offset (Fig. 3.1-1). This means extrusion of the middle block, situated between the Siglistorf anticline and BIH lineament, to the east, relative to the blocks in the north and south. Horizontal slip correlates with dip of the Siglistorf anticline that is large offset at steep portion of the fault and small offset at low-angle dip of the Siglistorf anticline (Fig. 3.1-1). The Siglistorf anticline and BIH accommodate N-S shortening due to thrust faulting (Fig. 3.1-1).

Uplift occurs throughout the whole model area (Fig. 3.1-1) due to the push from the south. Uplift increases towards the surface, but also piece-wise from the southern model boundary towards the BIH, from the BIH lineament to the Siglistorf anticline and from the Siglistorf anticline to the northern model boundary (Fig. 3.1-1). N-S shortening occurs with the BIH lineament and the Siglistorf anticline accommodating a portion of the shortening by thrust faulting (Fig. 3.1-1).

3.2 Stress field results of the base model

3.2.1 S_H orientations

The prevailing S_H orientation is 170-175° (Fig. 3.2-1). In the vicinity of the Siglistorf anticline S_H rotates by 5-10° counter-clockwise with some very local rotations to ~140°. No depth dependence of the S_H orientation is recognisable. This does not imply that there is no stress decoupling active in any of the formations, because the boundary conditions are uniformly applied over the whole depth extent of the model and in model BM there is no decoupling mechanism possible other than by the stiffness contrast between the individual formations.

The modelled S_H orientation agrees very well with the B-quality data record from the Weiach borehole with a S_H orientation of 172° between 560-2276 m drilled depth derived from 772 m borehole breakout length (Heidbach & Reinecker, 2013). A second C-quality data record for Weiach shows a S_H orientation of 134° representing the depth section 408-558 m drilled depth (42 m borehole breakout length; a few in the Wildegg Formation but most of these in the Upper Dogger above the Opalinus Clay). This local S_H orientation is not resolved in the model results.

3.2.2 Stress regime

The tectonic regime in model BM shows transgression to compression close to the surface, visualised in terms of the Regime Stress Ratio RSR (Simpson 1997; Fig. 3.2-2). In the deeper parts and also in the Opalinus Clay strike-slip regime prevails. The stratification is visible in the results with competent formations being somewhat more compressive than weak ones, indicating that the far field push is governed by the stiff formations. Relative extension south of the Siglistorf anticline near the western model boundary and relative compression south of the Siglistorf anticline near the eastern model boundary is the consequence of the 0.4 m pull at the eastern and western model boundaries perpendicular to the boundaries, while the Siglistorf anticline is left-laterally reactivated (Fig. 3.2-2).

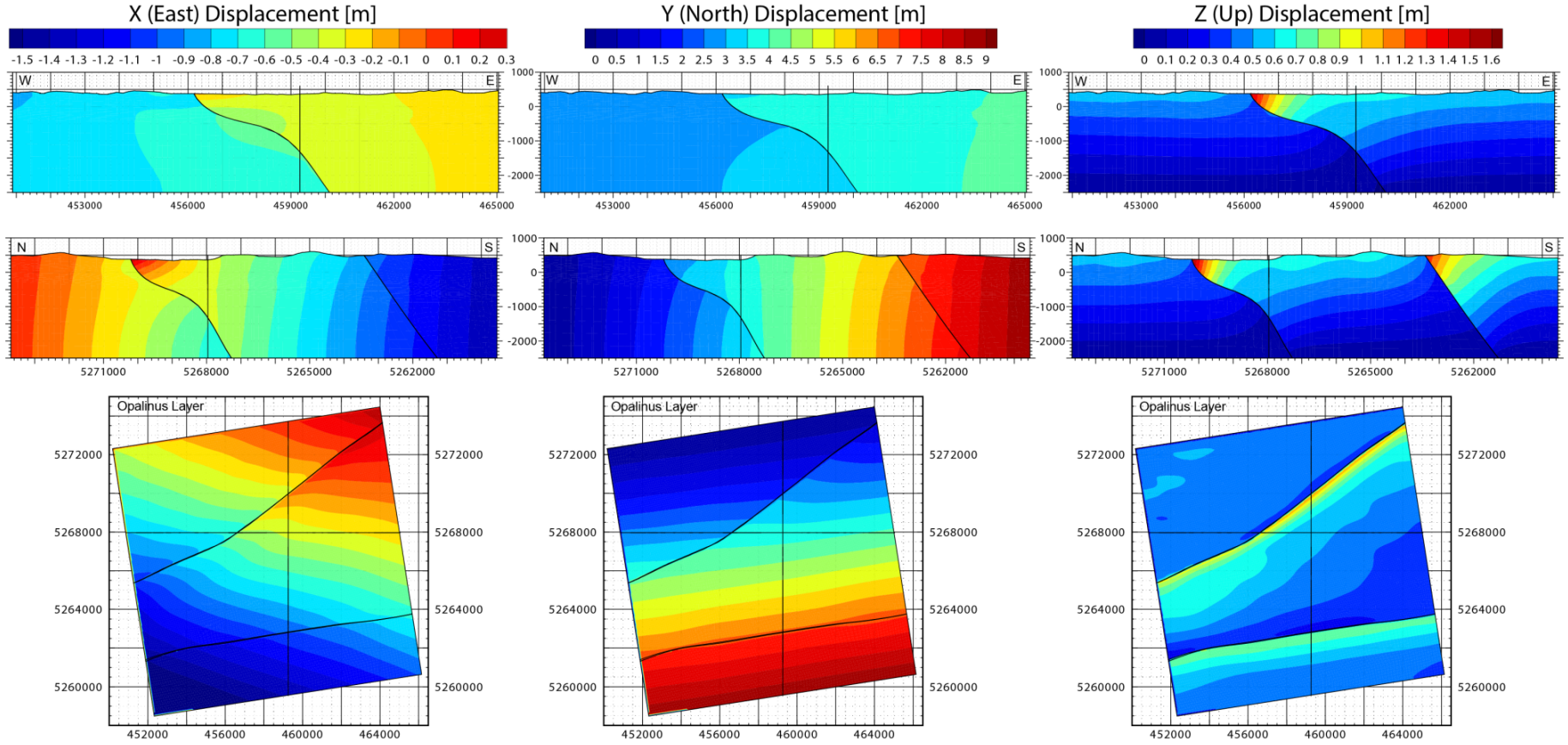

Fig. 3.1-1: Displacements in the base model BM.

EW (left column), NS (middle column) and vertical displacements (right column) in vertical EW (top row) and NS (middle row) profiles through the Weiach wellbore as well as in the middle surface of the Opalinus Clay (bottom row). Thin lines denote the location of the profiles.

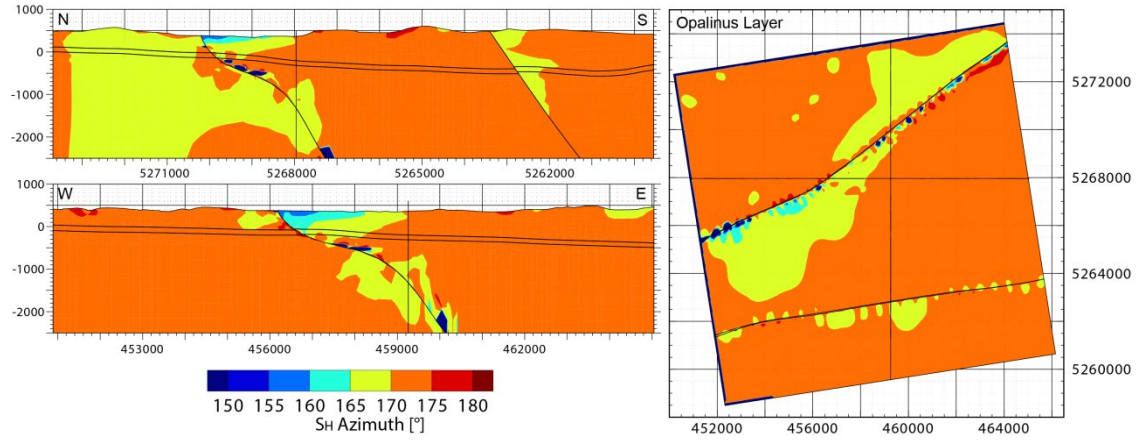

Fig. 3.2-1: S_H orientation of model BM.

NS and EW profiles through the Weiach wellbore (left) and in the middle surface of the Opalinus Clay (right). Thin lines denote the location of the profiles.

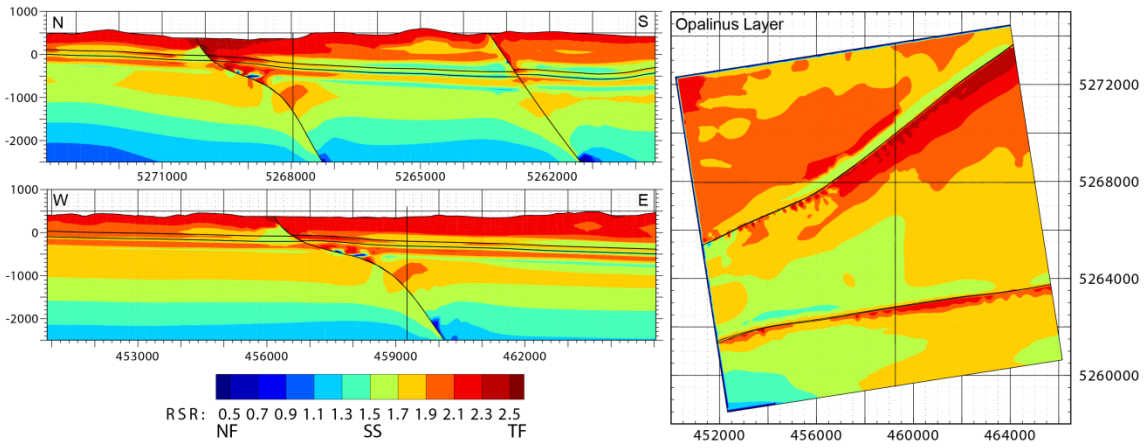

Fig. 3.2-2: Tectonic regime in terms of Regime Stress Ratio (RSR) of model BM.

RSR is a continuous value for the tectonic regime with NF=Normal Faulting, SS=Strike-Slip, TF=Thrust Faulting. Displayed is the RSR along NS and EW profiles through the Weiach wellbore (left) and in the middle surface of the Opalinus Clay formation (right). Thin lines denote the location of the profiles.

3.2.3 Stress ratios

The ratio S_H/S_h ranges between 1.2 and 1.4 in the Opalinus Clay in the area of interest, whereas S_H/S_h is greater between 1.4 and 2.2 in other formations (Fig. 3.2-3). Furthermore, S_H/S_h generally increases towards the surface. Again, individual formations are visible with S_H/S_h being higher in stiffer formations than in softer formations.

The ratio S_H/S_V exhibits high values > 2 in the uppermost Molasse but strongly decreases to 2 and below at greater depths (Fig. 3.2-3). The ratio S_H/S_V is about 1 at the base of the model, thus also the ratio S_H/S_V generally increases towards the surface. In the Opalinus Clay S_H/S_V ranges between about 1 and 1.5 in the area of interest[1], but mostly 1.1-1.3 with an increase in a narrow stretch of 1-2 km south of the Siglistorf anticline towards the fault (Fig. 3.2-3).

[1] Potential repository level, i.e. the area SW of the Siglistorf anticline and north of the BIH

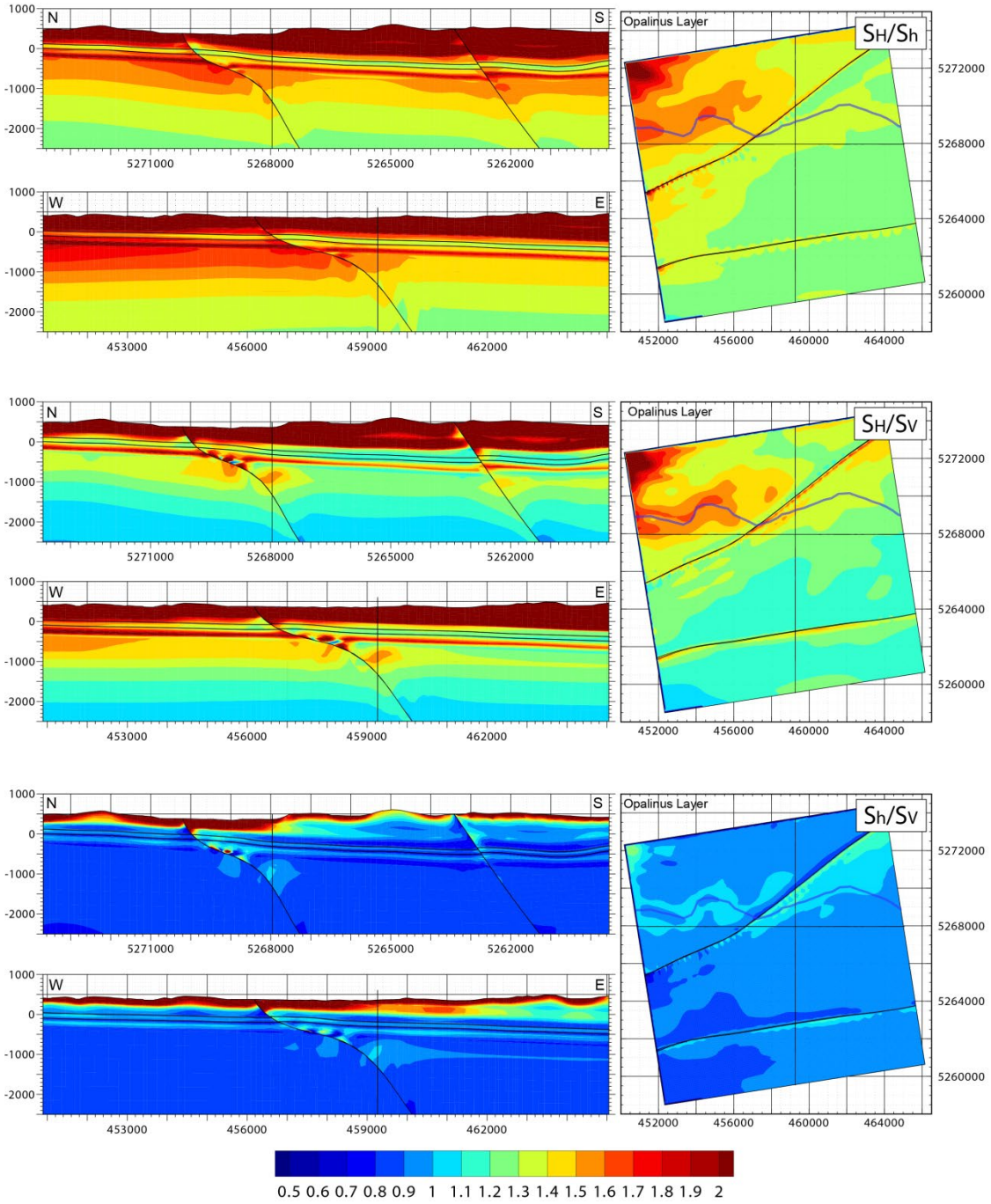

Fig. 3.2-3: Stress ratios of model BM.

Stress ratios S_H/S_h (top), S_H/S_V (middle) and S_h/S_V (bottom) in NS and EW profiles through the Weiach borehole (left) and in the middle surface of the Opalinus Clay formation (right). Note that colour scale is the same for all figures. Thin lines denote location of profiles. Blue line in the map views of the Opalinus Clay formation shows the Rhine river.

The ratio S_h/S_V varies between about 0.8 and 1.0 in the area of interest in the Opalinus Clay, but mostly S_h/S_V is slightly less than one. Also S_h/S_V increases towards the Siglistorf anticline (Fig. 3.2-3).

All stress ratios S_H/S_h, S_H/S_V and S_h/S_V show reduced values within the Opalinus Clay compared to the stiffer formations above and below (Fig. 3.2-3). Further, all stress ratios S_H/S_h, S_H/S_V and S_h/S_V tend to increase beneath topographic depressions, e.g. below the Rhine valley. Below valleys S_V is reduced due to the lower weight of the overburden and the horizontal stresses S_H and S_h are increased due to interaction between topography and far field push (see chapter 4.1). In the north of the model area stress ratios are generally higher in the Opalinus Clay than in the south. This is because stress ratios generally increase towards the surface (Opalinus Clay becomes shallower from south to north) because the vertical stress becomes zero at the surface, while the horizontal stresses S_H and S_h do not.

3.2.4 Differential stresses

The stiffer formations Upper Malm and Middle Muschelkalk are clearly characterised by increased differential stress of up to 20 MPa compared to low values in the softer formations (mostly < 6 MPa in the Opalinus Clay) (Fig. 3.2-4). The vertical changes of differential stress are therefore very pronounced (factor of about four), whereas within a formation differential stress is rather uniform (factor of about two at most), at least within the deeper formations (Fig. 3.2-4). Similarly, S_H-S_h is about < 7 MPa in the Opalinus Clay in the area of interest. The similarity of both stress differences denotes that $S_1 \cong S_H$ and $S_3 \cong S_h$.

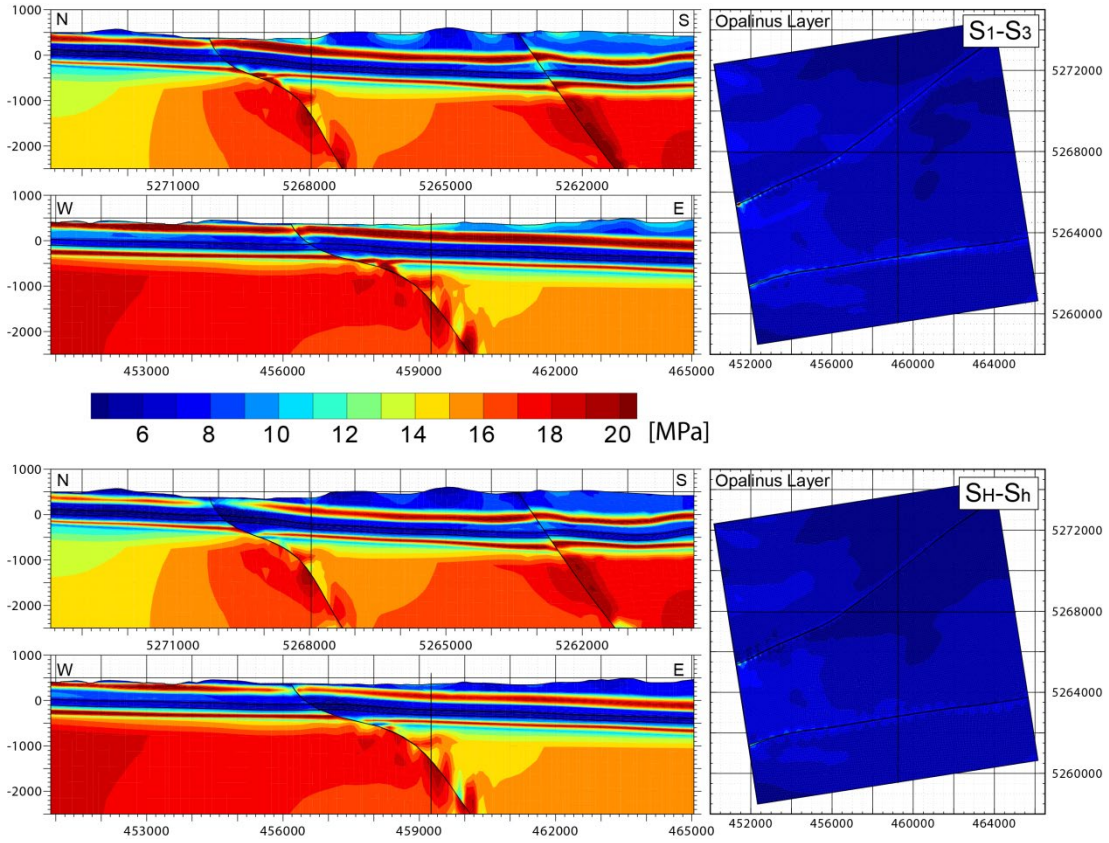

Fig. 3.2-4: Differential stresses of model BM.

Differential stress S_1- S_3 (top) and horizontal differential stress S_H-S_h (bottom) in vertical profiles through the Weiach borehole (left) and within the middle surface of the Opalinus Clay (right). Thin lines denote the location of the profiles.

4 Results of model variants

In this chapter the results of the model variants regarding fault geometry, fault friction, rock properties and an ice cover are described. Most of the model variants performed show only minor changes with respect to the BM. In the appendices A-C we present for all 15 model variants the three stress ratios S_H/S_h, S_h/S_V and S_H/S_V in overview figures at NS and EW profiles that cut through the location of the wellbore Weiach and further at the middle surface of the Opalinus Clay formation. In the following sections, based on these overview figure in the appendices we briefly summarize the key results and present, if reasonable, detailed or additional figures.

4.1 Imprints of topography

To investigate the influence of topography the homogeneous model E0 is considered because in this model the effect of topography is not concealed by the influence of the different elastic properties of the individual formations. Fig. 4.1-1 shows the magnitude of the maximum horizontal stress S_H of the initial stress (i.e. without tectonic boundary conditions applied) of the homogeneous model. While the pattern of topography appears in the vertical stress (not shown), it is hardly recognisable in S_H. Yet, already at shallow depth the influence of topography is no longer visible. Stresses in the homogeneous model E0 are dominated by the influence of the faults.

Contrarily, the pattern of topography is clearly expressed in S_H, once tectonic boundary conditions are applied. In this case S_H corresponds roughly to the NS component of stress (Fig. 4.1-2). Stress is increased below valleys, particularly below EW elongated ones, while stress is reduced below mountains. The tectonic far field stresses induce compressional stresses in topographical depressions and extension in topographic highs. The topographical influence on stress can be traced down to several hundred metres depth, the Rhine valley in the northwest down to sea level. Particularly, high gradients of topography are expressed in the stress pattern. E.g. at the northern rim of the mountain range between Weiach and Zweidlen elevation increases by 150 m from north to south within a distance of only 200 m and this results in a stress difference of c. 4 MPa at 200 m above sea level (i.e., at 170 and 320 m depth, respectively). The marked spot of increased stress 2.5 km SW of Weiach also results from steep slopes bordering a small valley where elevation is 420 m at Hueb/Talmüli and 550 m just 250 m to the north and south, respectively, resulting in a stress difference of c. 10 MPa at 400 m a.s.l. (i.e. 20 and 150 m depth, respectively). However, the effect of small wave-length gradients disappear at shallower depth than elevation changes of greater lateral extent.

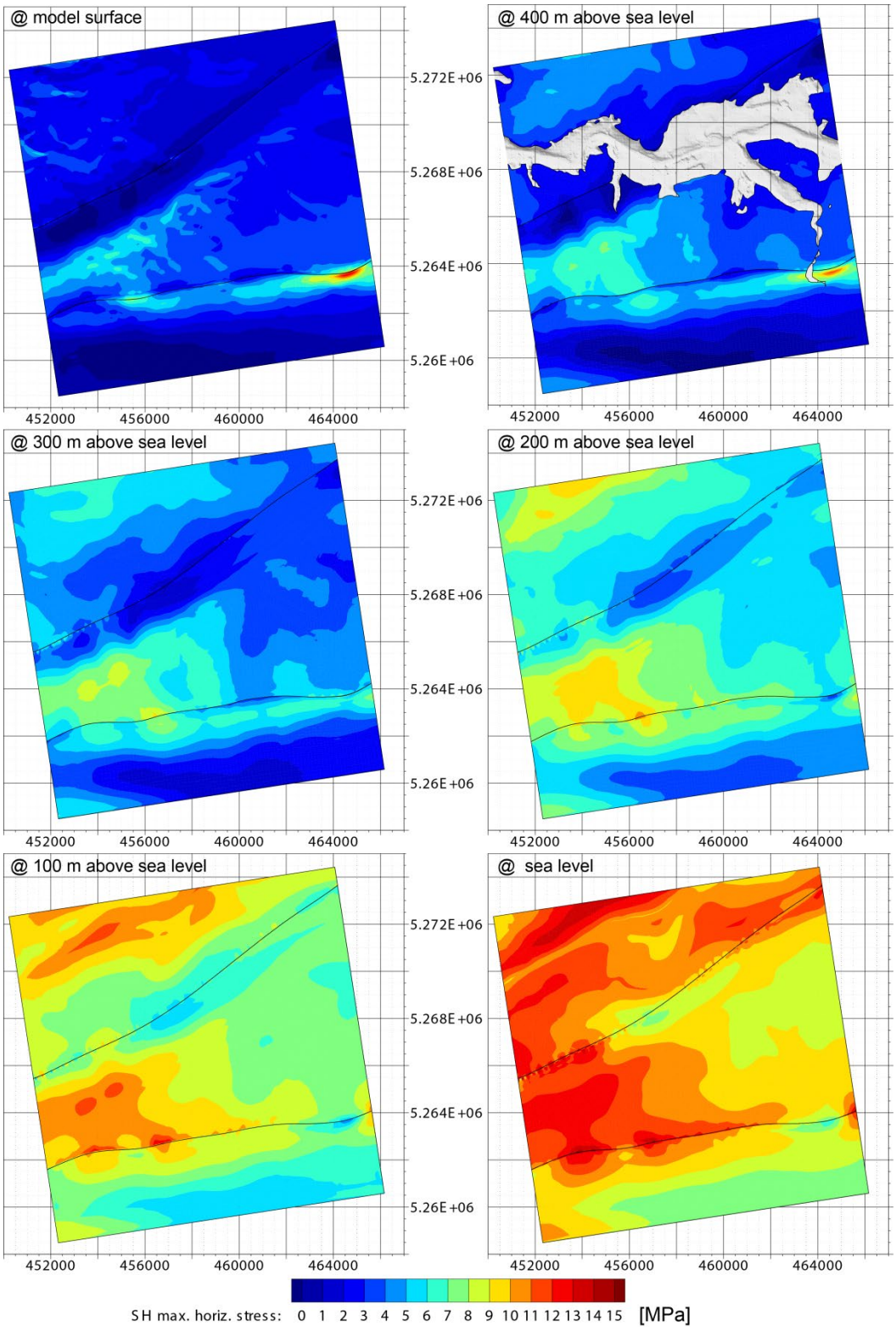

Fig. 4.1-1: S_H magnitude of initial stress from the homogeneous model E0.

S_H magnitude of initial stress only (that is the stress state only due to gravity, i.e. without tectonic boundary conditions) of model E0 with homogeneous elastic properties and density is shown at different depths.

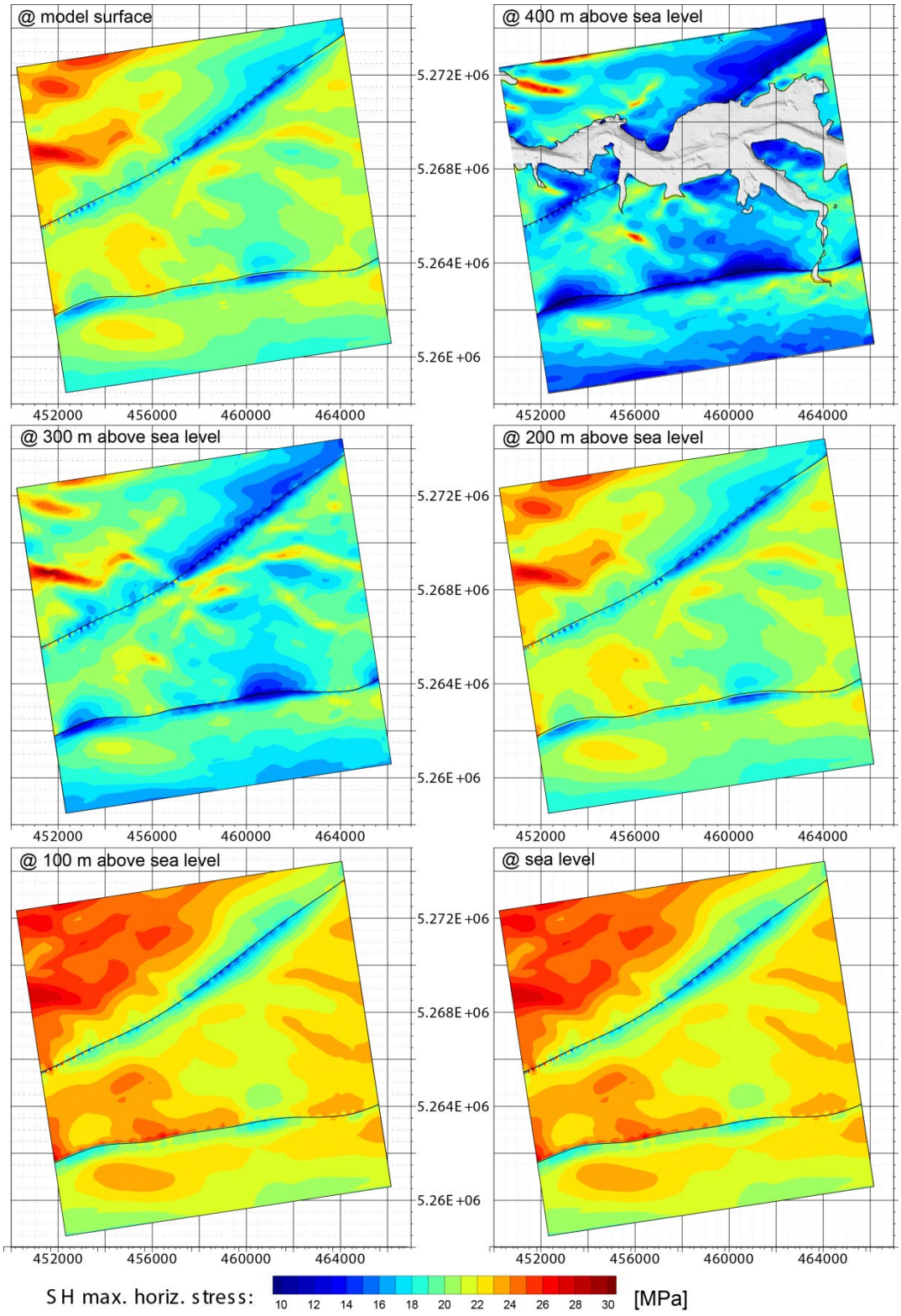

Fig. 4.1-2: S_H magnitude from the homogeneous model E0.

S_H magnitude from the homogeneous model E0 resulting from initial stress plus tectonic stress at different depths show the influence of topography and the lateral compression due to the kinematic boundary conditions.

4.2 Influence of rock properties

The homogeneous model E0 shows a clear increase of S_h/S_V by up to 0.3 in the middle of the Opalinus Clay with respect to BM, particularly in the north (App. C-3). This is because S_V in the homogeneous model is similar to the inhomogeneous model (average density in the above lying formations is similar) but S_h is greater because the Young's modulus in E0 is 25 GPa compared to 10 GPa in the Opalinus Clay in BM, which results in higher horizontal stress at a given push at the southern model boundary. Also S_H/S_h is strongly increased in E0 by about 0.3-0.5 with regard to BM (App. A-3, Fig. 4.2-1).

Increased or decreased Young's moduli in the Lias and Upper Mittelkeuper and in the Upper Dogger below and above the Opalinus Clay, respectively, hardly affect S_H/S_h, S_h/S_V and S_H/S_V in the Opalinus Clay (Models E1-E4 in App. A-3, B-3, C-3, Fig. 4.2-1). In E1 and E3 the stress ratios are slightly increased and in E2 and E4 slightly decreased compared to BM, with changes being most pronounced in E2 and E3, but smaller than 0.1.

Plastic rock behaviour as it is incorporated in model P1 does not result in any significant changes of stress ratios compared to BM. This is because the strength of rock is not reached throughout most of the model so that no plastic strain developed and therefore no stress change compared to the elastic model can be seen. Plastic strain only occurs at some locations at the bottom or at edges of the model, particularly, where they are intersected by faults.

4.3 Influence of fault and friction coefficient

Incorporation of the backthrust fault reduces stress outside the wedge formed by the backthrust and the Siglistorf anticline. The decrease of the stress ratios S_H/S_h, S_h/S_V and S_H/S_V within the Opalinus Clay compared to BM predominantly occurs right beside the wedge but also north of the wedge up to the northern model boundary, however the decrease of stress ratios is <0.1 at greater distance from the wedge. The uplift of the wedge generates space which lowers horizontal stress in the individual formations. In the Opalinus Clay the effect of the backthrust is smaller than at shallower depth because the wedge ceases at about the depth of the Opalinus Clay and gets broader towards the surface. Particularly, horizontal stress anisotropy is reduced by the backthrust in the Upper Malm south of the Siglistorf anticline (App. A-2 S_H/S_h N-S profiles).

The model without faults in the basement (GB; more precisely: hardly active faults in the basement due to very high coefficient of friction with μ'=100) reduces the stress ratios S_H/S_h, S_h/S_V and S_H/S_V within the Opalinus Clay in most of the model area. In the formations below S_H/S_h increases. However, changes compared to BM are smaller than 0.1.

Model GE incorporating a frictional contact surface in the middle surface of the Middle Muschelkalk shows quite different results than all other models. This is only in part due to the incorporated contact surface that should represent a detachment horizon. In this model modified boundary conditions were applied as the northward directed push was not applied on the whole southern model boundary but only above that contact surface. Therefore, below that contact surface horizontal stress and hence the ratios S_h/S_V and S_H/S_V are smaller than in the other models (App. B-2, C-2). Above the Middle Muschelkalk stress ratios are strongly increased south of the BIH, whereas north of it stress ratios are smaller by 0.1-0.3 compared to BM. S_H/S_h becomes nearly one over wide areas in the Opalinus Clay (App. A-3), which is an almost transversally isotropic stress state. The stresses associated with the push are consumed in the block south of the BIH and are not well transferred across the BIH further to the north.

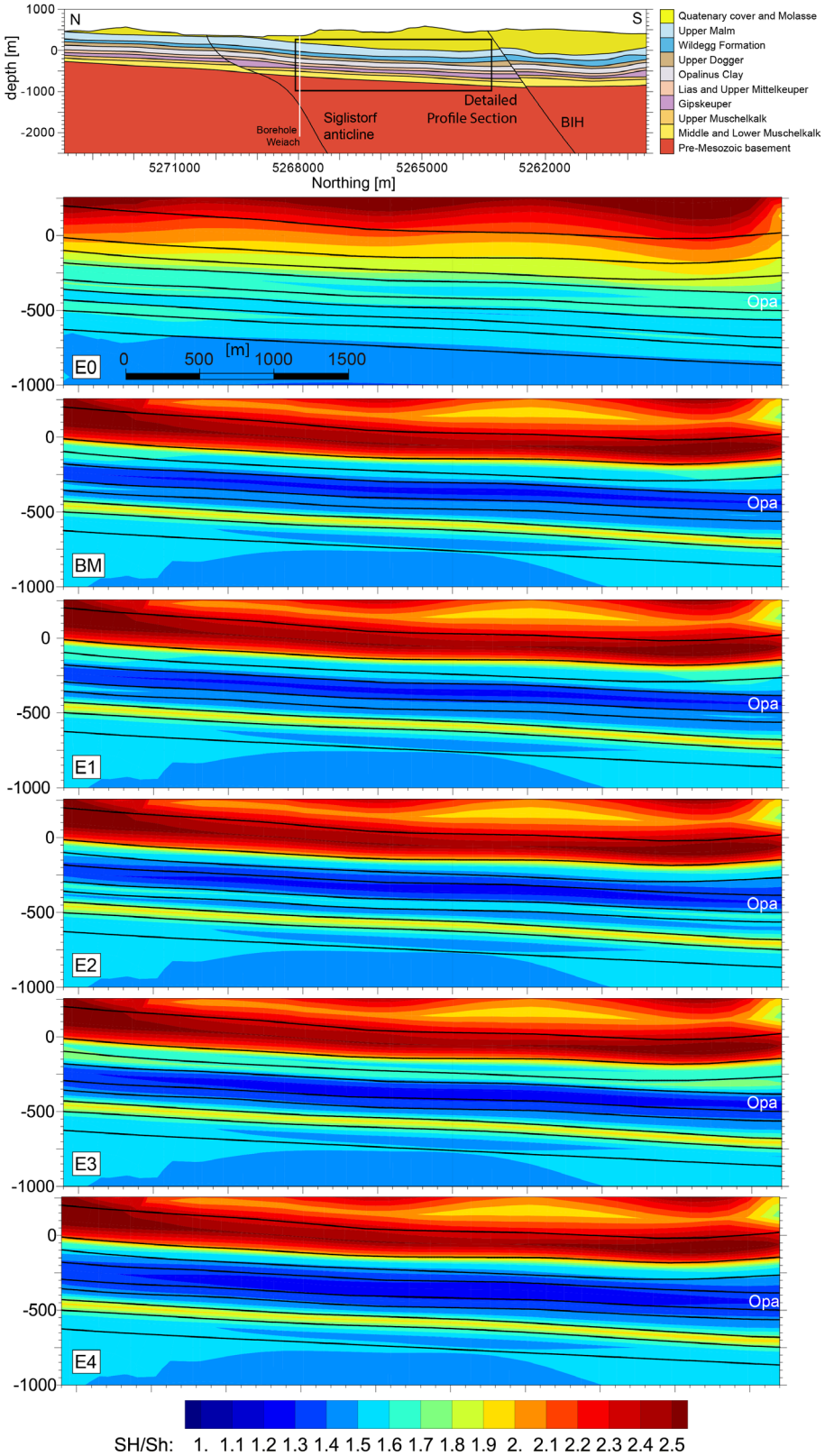

Fig. 4.3-1: Detailed view of S_H/S_h in NS profiles for different Young's moduli.
NS profiles cuts through the wellbore Weiach (for model abbreviations see Tab. 2.7-1).

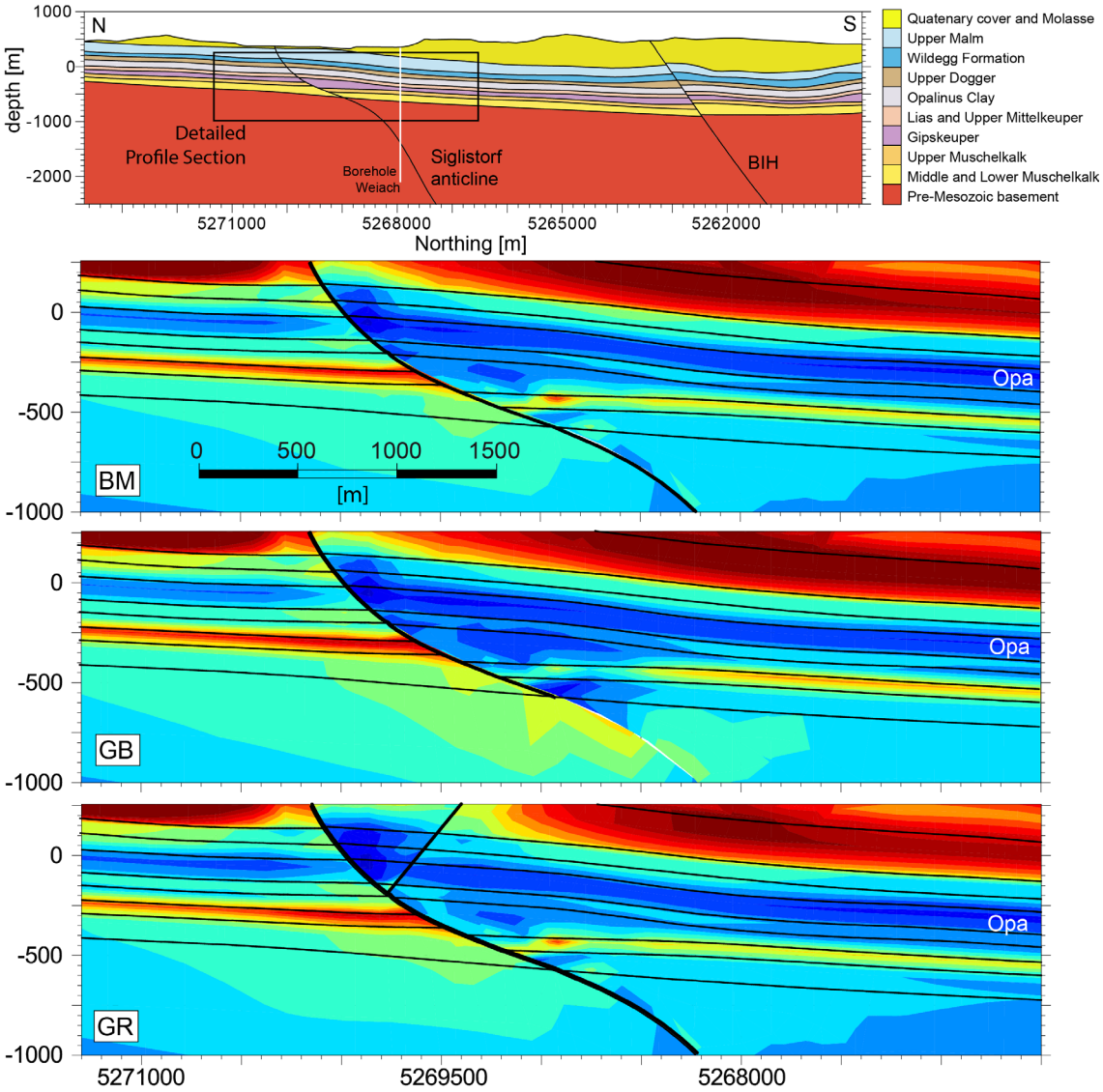

Fig. 4.3-2: S_H/S_h in NS profile for different fault geometries.

NS profile through wellbore Weiach for models with different configurations of the Siglistorf anticline (Model abbreviations are given in Tab. 2.7-1). Box in the upper figure shows location.

Models with increased effective coefficient of friction (R06 and R10) compared to BM result in increased S_H/S_h and S_H/S_V but decreased S_h/S_V in the Opalinus Clay, except in the western and southern part of the middle block between BIH and Siglistorf anticline, where S_h/S_V also increases (App. A-3, B-3, C-3). Changes are mostly smaller than 0.1, but become 0.2 right south of the Siglistorf anticline in the eastern half of the model.

Higher fault friction increases horizontal stress anisotropy S_H/S_h, which can be best recognized in the NS profile through the location of the Weiach wellbore (App. A-2). From about half a kilometre north of the Siglistorf anticline to about 2 km south of the Siglistorf anticline S_H/S_h is increased by about 50% in the Upper Malm (S_H/S_h up to 2.5) compared to BM. The ratio S_H/S_h is also increased south of it although less. Since the coefficient of friction governs the coupling between the blocks involved and their ability to be reactivated, this indicates that the EW strik-

ing faults weaken the push from the far field and reduce horizontal stress anisotropy. In turn, without these faults the push from the far field is more efficiently transferred.

4.4 Ice cover

An ice cover reduces the stress ratios S_H/S_h, S_h/S_V and S_H/S_V, particularly at the surface and at shallow depths (App. A-2, B-2, C-2), but also in the Opalinus Clay (App. A-3, B-3, C-3). In model I500, where ice is locally absent and present only in valleys below 500 m elevation, this effect is not as pronounced as in models I500s and I1000 where the ice cover is 500 m and 152-684 m thick, respectively. The stress ratios for models I500s and I1000 are similar, which indicates that the mean thickness of ice is more important for the stress conditions at the depth of the host rock than local variations of ice thickness.

S_H/S_V and S_h/S_V are more decreased by the ice cover than S_H/S_h. This is because at the surface S_V is zero while S_H and S_h are not and therefore the ratios S_H/S_V and S_h/S_V are strongly altered if a load acts on the original surface. The reduction of S_H/S_h and S_h/S_V due to the ice cover amounts to 0.1-0.3 in the Opalinus Clay in models I500s and I1000 and of S_H/S_h mostly less than 0.1. Furthermore, the stress ratios in the presence of an ice cover show reduced spatial variability in the Opalinus Clay compared to BM, particularly S_h/S_V becomes rather uniform.

5 Discussion

5.1 Implications of results

5.1.1 What is the role of the faults on the stress and displacement field?

Based on the model results it can be said that the major EW striking Siglistorf anticline and the BIH fault weaken the northward directed push from the far field within the sedimentary cover. This is revealed by comparison of the BM with those model variants in which higher coefficients of friction are attributed to the faults (R06 and R10), thereby reducing their ability to slip at a given stress state and the end member case of infinite friction would mean a fault is absent. The models with high friction on the faults show higher S_H/S_h ratio than the BM, which is an expression of higher horizontal stress anisotropy due to the push at high fault friction. Model GE is the most prominent example for the weakening influence of the faults on the push as S_H/S_V and S_h/S_V are strongly reduced at the BIH.

Several mechanisms can be identified for the weakening of the push and the associated reduction of horizontal stress anisotropy in the Mesozoic formations. 1) The faults are reactivated by thrust faulting (Fig. 3.1-1). The shortening as a result of thrust faulting reduces S-N directed compressional stress. 2) The thrust faulting results in vertical offset of the Mesozoic formations at the faults. If due to this vertical offset a competent and a weak formation lie at opposite sides of the fault at a certain depth, the efficiency of the S-N directed push is diminished because the push is governed by the competent formations. 3) The faults are also laterally reactivated (Fig. 3.1-1). The lateral reactivation of faults, with right-lateral slip on the BIH and left-lateral slip on the Siglistorf anticline, results in an eastward directed extrusion of the block between the Siglistorf anticline and the BIH, thereby also weakening the S-N directed push.

5.1.2 What is the role of the individual formations?

The northward directed push from the far field is carried predominantly by the formations of high stiffness. While deformation is widely the same in the individual Mesozoic formations due to the uniformly applied displacement at the southern model boundary over the whole depth extent of the model, stress regime (RSR) and the various stress ratios S_H/S_h, S_H/S_V, S_h/S_V as well as horizontal differential stress S_H-S_h are higher in the stiffer formations than in the softer formations. In some sense the stiff Upper Malm as well as Middle and Lower Muschelkalk formations embracing the clay-mineral richer formations in between shield the latter, leaving them in a stress shadow. However, strength of the softer formations is much lower than strength of the stiff formations, thus not necessarily the stiff formations fail first as deformation increases.

Similarly, the stiffness values of the Upper Dogger and Lias and Upper Mittelkeuper lying right above and below the Opalinus Clay affects stress ratios in the Opalinus Clay. With reduced stiffness both, above and below the Opalinus Clay (E4) the stress ratios within the Opalinus Clay are reduced the most among the cases considered, with S_H/S_h approaching 1.1 (Fig. 4.2-1). This is because the formations of reduced stiffness above and below accommodate the high stresses from formations above and below by deformation, thus reducing stress anisotropy in the Opalinus Clay. In turn, stiffer Upper Dogger and Lias and Upper Mittelkeuper (E1) result in increased stress ratios in the Opalinus Clay (Fig. 4.2-1). Reduction of stress ratios in the Opalinus Clay is more effective if stiffness of Upper Dogger is increased and stiffness of the Lias and Upper Mittelkeuper decreased than vice versa (E2 and E3 in Fig. 4.2-1, respectively). However, changes of S_H/S_h among the different cases considered amount to 0.1 at most.

5.1.3 How far do the faults influence the stress field?

An important question is at what distance from the faults the state of stress can be assumed as being undisturbed by the faults. The role of the faults lowering the overall compression exerted by the push from the far field was outlined already. This effect is appreciable throughout the whole area of the model. In addition, there is a near field discernible in which stress is altered by the faults with respect to the stress state at greater distance from the faults. This near field extends to approximately 1-2 km from the faults in the models considered. Generally, the distance at which a fault affects stress in its surrounding depends on the coefficient of friction and total fault displacement, but also on the geometric complexity (radius of bends and curvature of the fault). Stress concentrations, if present, predominantly occur nearby faults and are geometry induced.

5.1.4 Are there hints for stress concentrations in the geological siting region NL?

Stress concentrations, i.e. large changes of the stress state in the host rock, could assist in designating potentially tectonically affected zones. High stress changes predominantly appear close to faults (see discussion on dependency of stress on distance from the fault). At this point, it should be noted that this depends strongly on fault geometry and it is not clear whether the widely generic faults in the model represent the actual structures adequately. Stress concentrations close to the edges of the model or where faults intersect the model boundaries can be artefacts and are not reliable. Stress concentrations of topographical origin are strong only near the surface.

5.1.5 What is the role of the coefficient of friction on faults?

The higher fault friction, (a) the smaller are displacements at the faults (both thrust and horizontal components, thus the push is less weakened than at small fault friction; see explanation on "What is the role of the faults on the stress and displacement field?") and (b) the higher is S_H/S_h in the Mesozoic sediments, in particular in the uppermost 200-300 m within 2 km south of the Siglistorf anticline (App. A-1, A-2).

5.1.6 What is the role of the backthrust?

The backthrust reduces horizontal anisotropy (compare S_H/S_h of BM and GR, Fig. 4.3-1). However, the influence of the backthrust is very small at the depth of the host rock and increases towards the surface.

5.1.7 What is the role of topography and Quaternary sediment channels?

The direct effect of topography due to the laterally varying weight acting on the subsurface and the associated increase of stress below mountains and decrease below valleys is visible. However, in the model topography affects stress mostly in an indirect way. The northward directed push induces stress that is determined by the shape of the surface and that can be best understood in terms of bending stresses. Stress increases below valleys and decreases below mountains, thus this induced stress change is opposite to the stress change that originates from the weight of the overburden. The imprint of the Rhine valley can be traced down to about 500 m depth. In comparison with the topography the impact of the quatenary sediment channels is smaller as their density contrast to the Molasse sediment and spatial extend is significantly smaller and does not affect the Opalinus Clay formation.

5.1.8 What is the role of an ice cap?

An ice cap decreases the stress ratios S_H/S_h, S_h/S_V and S_H/S_V, particularly at shallow depths (App. A-2, B-2, C-2). Local variations of the stress ratios are reduced, particularly for the ratio S_h/S_V (App. C-3).

5.2 Impact of the initial stress field and boundary conditions

The implemented initial stress field (that balances the gravitational stress and provides an appropriate ratio of horizontal to vertical stress) that is applied to calibrate the model against the stress data using equation (5) and the kinematic boundary conditions used to calibrate the final stress state against the hydro-frac data from the wellbore Benken rely on few data only and is thus uncertain. We test in the following the impact of a slightly different initial stress field and different boundary conditions. The model BM_hi assumes in the first step of the initial stress field calibration (see section 2.5) a homogeneous distribution of ν=0.43 for all formations. Tectonic boundary conditions are 10 m push from South to North and no displacement perpendicular to the model boundary is allowed for the northern, eastern and western model boundaries.

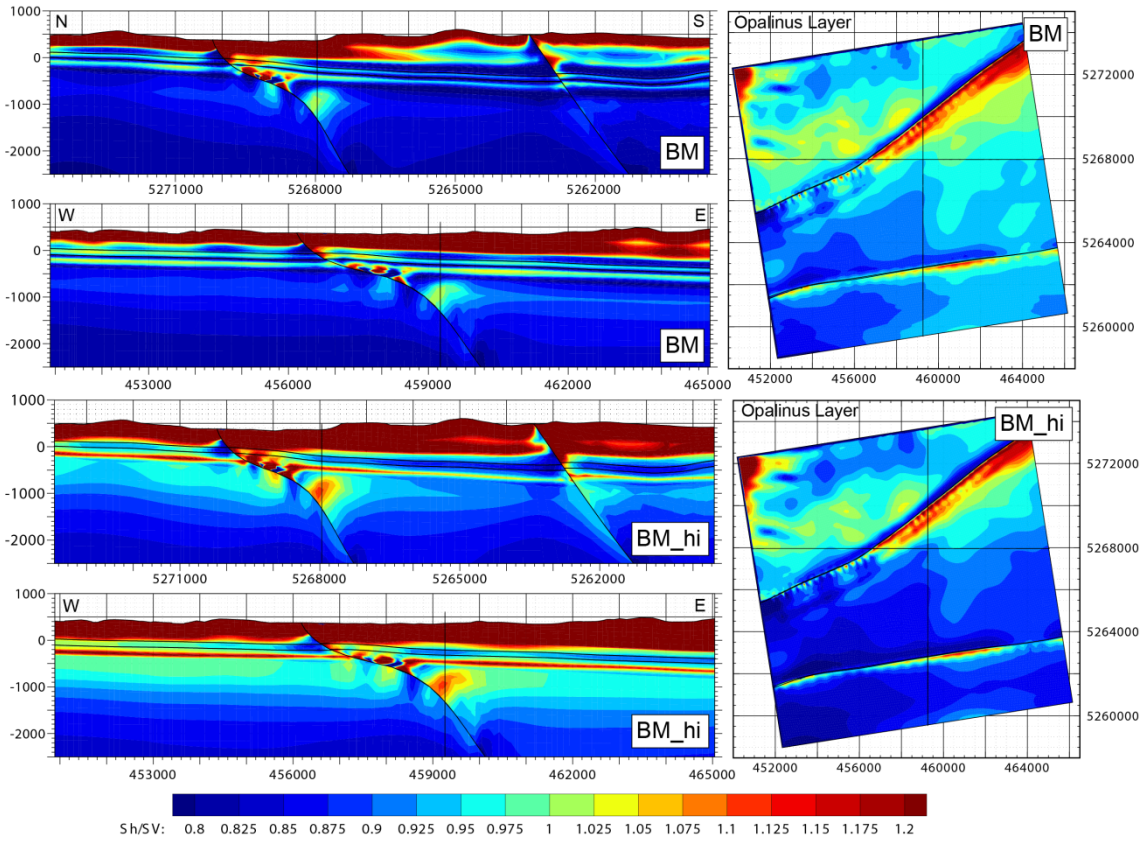

Fig. 5.2-1: Impact on S_h/S_V ratio due to changes in stress field calibration.

Top figures show S_h/S_V of the model BM in N-S and E-W profiles. Bottom figures show S_h/S_V of the model BM_hi where in the initial stress field calibration step (for technical details see Section 2.5) a Poisson's ratio of ν=0.43 is assumed, 10 m push and no pull at the sides for the tectonic stress field implementation. Thin lines in the profiles show top and bottom of the Opalinus Clay formation. Thin lines denote the location of the profiles.

The resulting K-ratio in the Opalinus Clay at the wellbore Weiach is approximately 0.88, hence lower than K = 0.94 derived from the measurement. The impact on the competent formation is

even larger, with K-ratios clearly >1.0 (Fig. 5.2-1). However, the impact on the stress magnitudes is relatively small. The difference of the horizontal stress magnitudes S_H-S_h displayed in Fig. 5.2-2 reveals that the changes are only a few MPa. The observation that the competent formations carry most of the differential stresses imposed by the lateral tectonic forces remains unchanged.

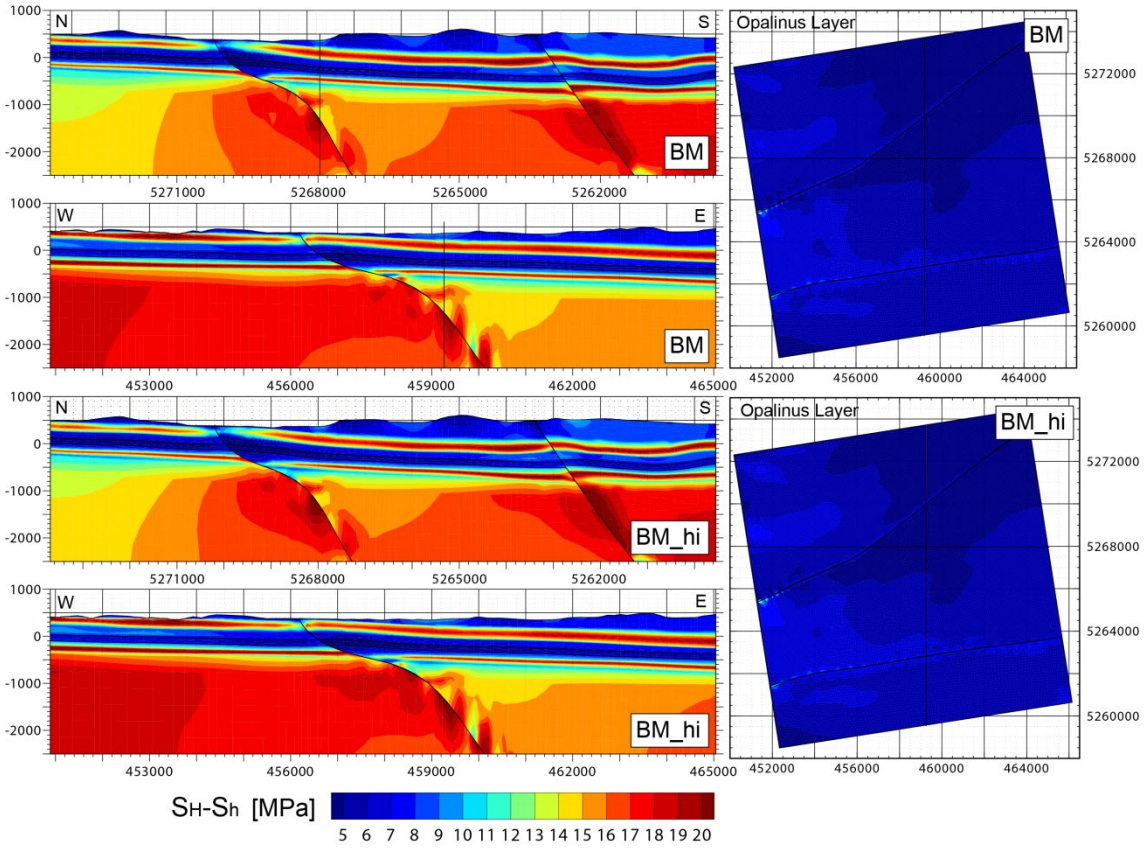

Fig. 5.2-2: Impact on S_H-S_h due to changes in stress field calibration.

Top figures show the results of the model BM. Bottom figures show the results of the model BM_hi where for the initial stress field calibration phase (details of the technical procedure are given in Section 2.5) a Poisson's ratio of ν=0.43 is assumed and 10 m push and no pull at the sides for the tectonic stress field implementation. Thin lines in profiles show top and bottom of the Opalinus Clay formation. Thin lines denote profile locations.

5.3 Pushing the model into the plastic limit

In the previous model runs the southern model boundary was displaced by 9m to the north (perpendicular to the boundary) to account for the tectonic boundary conditions, i.e. to generate the desired lateral in situ stress magnitudes for the Opalinus Clay (chapters 2.5 and 2.6). As mentioned in chapter 4.2 and documented in Appendices A to C by the model variant P1, this rather moderate amount of shortening did not lead to failure in any of the geomechanical units. In this chapter the effect of further N-S shortening is assessed by starting with the model variant P1 (i.e. elasto-plastic behaviour in the bulk volume and material properties as specified in the last two columns of Table 2.7-1) and sequentially adding up to 21m of additional shortening (30m in total) and allowing for additional extension both at the western and eastern model boundaries by 1.1 m each (1.5 m total). The results of this model variant P2 are illustrated in Figs. 5.3-1and 5.3-2, and in Appendix D.

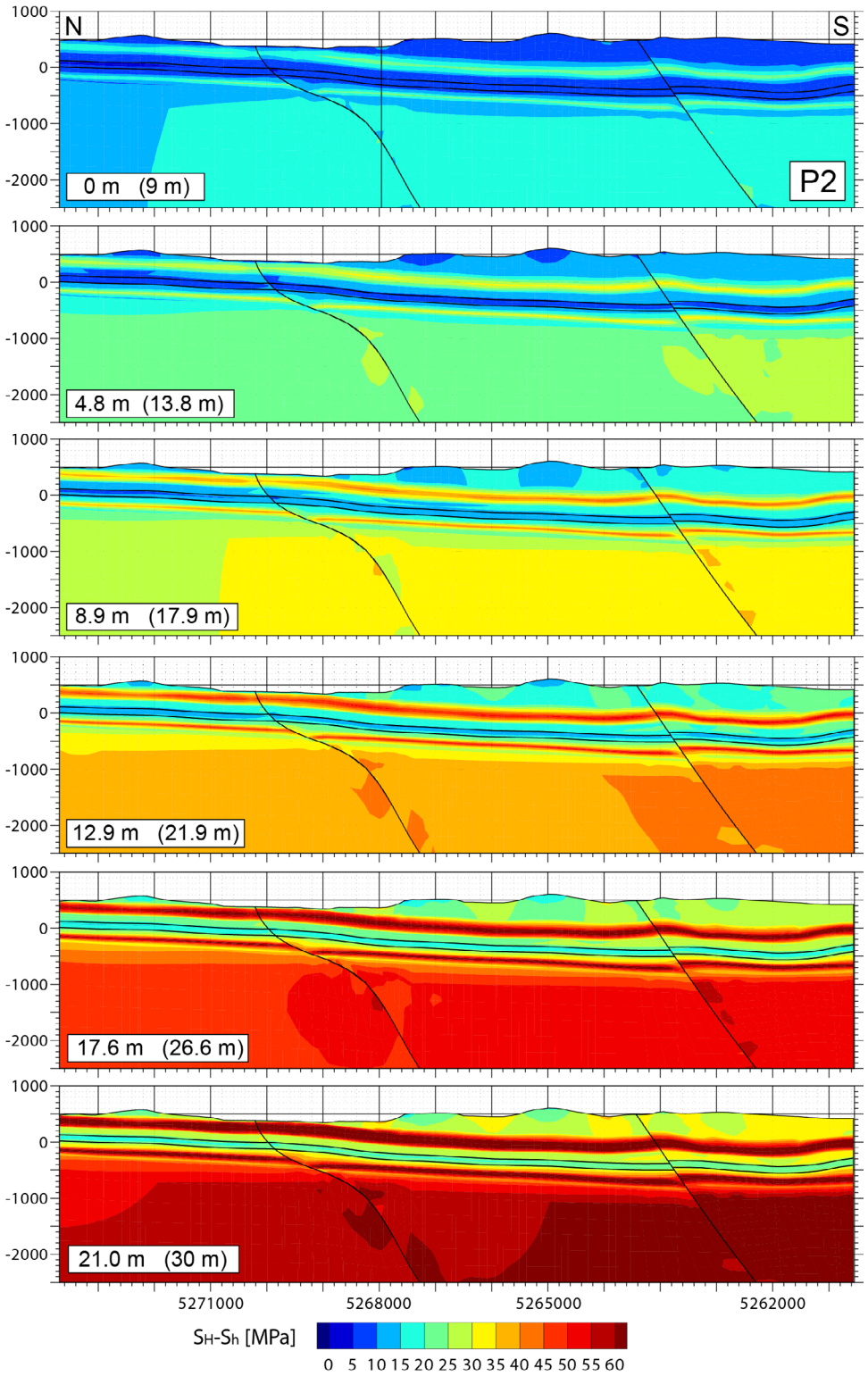

Fig. 5.3-1: Evolution of S_H-S_h with progressive NS shortening.

Indicated in the various NS cross sections is the amount of additional shortening with respect to model variant P1, with the total NS shortening (including P1) in brackets. Pull at the sides is increased linearly to 1.5 m on each side. Thin black lines indicate top and bottom of the Opalinus Clay.

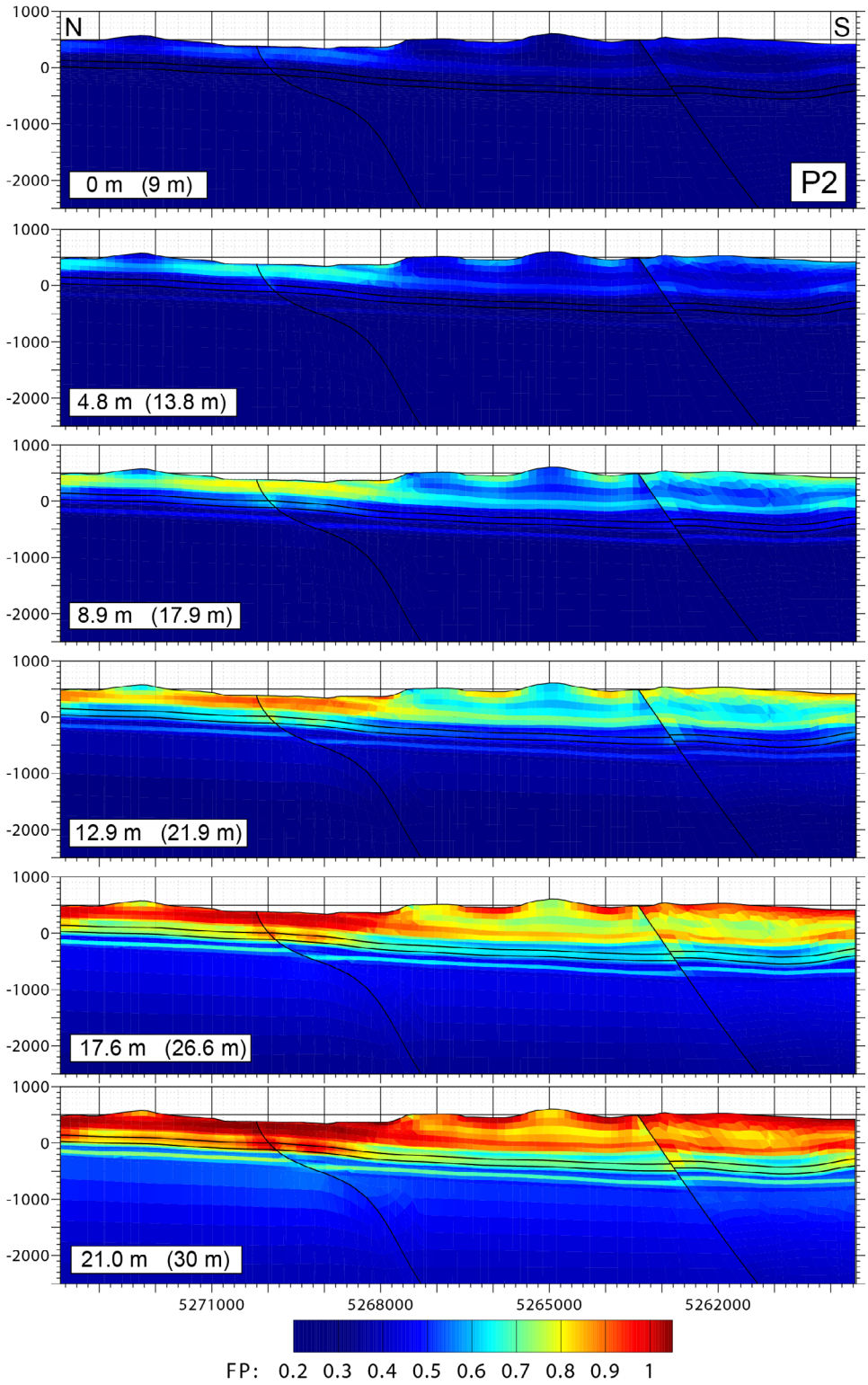

Fig. 5.3-2: Evolution of Fracture Potential (FP) with progressive NS shortening.

Indicated in the various NS cross sections is the amount of additional shortening with respect to model variant P1, with the total N-S shortening (including P1) in brackets. Pull at the sides is increased linearly to 1.5 m on each side. Thin black lines indicate top and bottom of the Opalinus Clay layer.

Assuming that the overall N-S shortening between the central Alps and the southern Black Forest north of the geological siting region is c. 1 mm/a, the N-S shortening within the model area is approximately 0.1 mm/a. Thus 21 m may broadly represent a time span of approximately 210 ka of shortening.

Fig. 5.3-1 shows the evolution of the horizontal differential stress at different time steps. The results show that the stiff formations of the Upper Malm and the Upper Muschelkalk bear most of the differential stress accumulation and the plastic limit is reached in particular where the competent formations are closer to the surface. This is visualized with the fracture potential value

$$FP=\sigma_d/\sigma_{dcrit} \quad (6)$$

With σ_d the differential stress and σ_{dcrit} the critical differential stress when the failure envelope is reached. Thus plastification starts when FP=1. This plastic limit is only reached after approximately 15 m of additional shortening where the FP value is close to or equals one (Fig. 5.3-2). In the Opalinus Clay formation FP values are not higher than 0.8 except near the Siglistorf anticline where FP values are close to one at the final stage with 21 m further N-S shortening (Fig. 5.3-2).

The Opalinus Clay has maximum values S_H-S_h< 20 MPa whereas the stiffer formations reach values S_H-S_h > 60 MPa. In Appendix D the evolution of the ratios S_H/S_h, S_H/S_V and S_h/S_V as well as the FP evolution is displayed as a map view on the mean layer of the Opalinus Clay formation. North of the Siglistorf anticline FP values reach one indicating that failure is reached for Opalinus Clay in this region. The ratios show a much greater increase in the NW corner of the model where burial depth of the Opalinus Clay is only a few hundred meters. Within the geological siting region NL, the model runs indicate that even after shortening of more than three times the amount used in the model P1 Opalinus Clay is only close to failure (FP > 0.9) in localized areas in the vicinity of the Siglistorf anticline.

5.4 Limitations and perspectives

The presented model includes a number of assumptions and simplifications to maintain practicability and due to lack of information on the subsurface. These assumptions and simplifications may pose limitations regarding the applicability and reliability of the model.

The faults included are merely generic structures. There is no clear evidence that the Siglistorf anticline and BIH lineament which are supposed to be structures within the sedimentary cover, penetrate the Pre-Mesozoic basement, except that deep rooted faults bordering the Permo-Carboniferous Trough may exist below. The BIH lineament is not a fault that penetrates the entire column of Mesozoic sediments from surface to basement in a single through-going plane of uniform dip (Chapter 2.2). The geometry of the Siglistorf anticline may be different than constructed, e.g. it may mouth in a listric way into one of the Mesozoic formations (Fig. 2.2-2). Finally, the backthrust of the Siglistorf anticline is a generic structure.

The simplifications also concern the model boundaries and the applied conditions at these. The model ends north of the Jura main thrust. Therefore, the influence of the geometrical peculiarities of this thrust altering the far field push, are not considered. A potential existence of prolonged hercynic striking faults extending from the Black Forest to below the Molasse Basin was neglected.

Below the Mesozoic sediments it was assumed that there is a uniform Pre-Mesozoic basement down to the model boundary at 2500 m b.s.l. Thus, we do account for a possible Permo-Carboniferous Trough and a crystalline basement, although in the Weiach borehole the contact between Pre-Mesozoic basement and the crystalline basement was encountered at 2020 m

depth. The exact boundaries of the Permo-Carboniferous Trough are not known and it is possible that the thickness of the Pre-Mesozoic basement varies strongly over the model area and they may even be absent at some parts of the area (Nagra, 2008).

The boundaries of the model are rather close to the geological siting region to be modelled. Therefore, boundary effects potentially affect the results. In particular, boundary conditions at the eastern and western model boundaries are difficult to define at the intersections of the faults with the model boundaries. As the Siglistorf anticline and BIH are reactivated left- and right-laterally, respectively, the boundaries should be defined accordingly, allowing fault slip at the boundaries. However, once fault slip is defined at the boundaries, fault slip is no longer an independent result of the model and it is unclear what amount of slip should be imposed. In turn, if no boundary-perpendicular fault slip is allowed at the model boundaries, which is the case for the model presented, an artefact comes into the model as artificial EW compression is generated at the eastern model boundary south of the Siglistorf anticline and extension at the western model boundary south of the Siglistorf anticline.

The parameters defining the plastic properties of the individual formations in case of the models P1 and P2 were chosen according to best knowledge. In principal plastic failure only occurs in layers close to the surface and in the vicinity of the Siglistorf anticline when substantial additional push is added to the model BM (Fig. 5.3-2, App. D). However, plastic failure may emerge earlier if boundary conditions at the southern model boundary would be defined differently, similar to the boundary conditions applied in model GE with push only above the Middle Muschelkalk.

The absence of data on stress magnitudes within the model area limits the reliability of the absolute stresses resulting from the model. If available, stress magnitude data could serve as calibration data. The assumption made that the reference stress and the tectonic load are the same in Weiach as in Benken, where stress magnitude data are available, is critical. While below Benken there are no Permocarboniferous sediments between the Mesozoic sediments and the crystalline basement, below Weiach Pre-Mesozoic sediments are encountered. Benken potentially rests on a crystalline horst structure whereas Weiach is situated above the Permo-Carboniferous Trough.

While the presented model results are reliable from a generic point of view in the sense that the effects of particular parameters of the model on the resulting stress state can be studied, uncertainty remains whether the model input is suitable to predict in situ stress reliably. In particular, model assumptions, chosen rock properties, interpreted fault geometries, remnant stress from the geological history, appropriate initial stress and boundary conditions are factors that are difficult to assess.

6 References

Altmann, J., Müller, T., Müller, B., Tingay, M. & Heidbach, O. (2010): Poroelastic contribution to the reservoir stress path, Int. J. of Rock Mech., 47, 1104-1113, doi:1110.1016/ j.ijrmms.2010.1108.1001.

Anderson, E. M. (1905): The dynamics of faulting, Trans. Edin. Geol. Soc., 8, 387-402.

Bercovici, D., Ricard, Y. & Richards, M. A. (2000): The Relation Between Mantle Dynamics and Plate Tectonics: A Primer, in The History and Dynamics of Global Plate Motion, edited by M. A. Richards, R. G. Gordon & R. D. van der Hilst, pp. 5-46, American Geophysical Union, Washington, D.C.

Brooker, E.W. & Ireland, H.O. (1965): Earth pressures at rest related to stress history. Canadian Geotechnical Journal 11/1, 1-15.

Célérier, B. (1995): Tectonic regime and slip orientation of reactivated faults, Geophys. J. Int, 121, 143-161.

Deichmann, N. (2010): Earthquakes in Switzerland and surrounding regions 1996-2009, pp., Swiss Seismological Service - ETH Zürich.

Diebold, P., Naef, H. & Amman, M. (1991): Zur Tektonik der Zentralen Nordschweiz: Interpretation aufgrund regionaler Seismik, Oberflächengeologie und Tiefbohrungen. Textband. Nagra Technischer Bericht. NTB 90-04. Nagra, Baden.

Engelder, T. (1992): Stress Regimes in the Lithosphere, 457 pp., Princeton, NJ.

Ferrari, A., Favero, V., Manca, D. & Laloui, L. (2012): Geotechnical characterizazion of core samples from the geothermal well Schlattingen LSA-1. Nagra Arbeitsbericht. NAB 12-50. Nagra, Wettingen.

Friedmann, M. (1972): Residual elastic strain in rocks, Tectonophysics, 15, 297-330.

Heidbach, O., Tingay, M., Barth, A., Reinecker, J., Kurfeß, D. & Müller, B. (2010): Global crustal stress pattern based on the World Stress Map database release 2008, Tectonophysics, 482(1-4), 3-15, doi:10.1016/j.tecto.2009.1007.1023.

Heidbach, O. & Reinecker, J. (2013): Analyse des rezenten Spannungsfeldes der Nordschweiz. Nagra Arbeitsbericht. NAB 12-05. Nagra, Wettingen.

Heidbach, O., Reinecker, J., Tingay, M., Müller, B., Sperner, B., Fuchs, K. & Wenzel, F. (2007): Plate boundary forces are not enough: Second- and third-order stress patterns highlighted in the World Stress Map database, Tectonics, 26, TC6014, doi:10.1029/ 2007TC002133.

Henk, A. (2008): Perspectives of Geomechanical Reservoir Models - Why Stress is Important, European Maganzine, 4, 1-5.

Hergert, T. & Heidbach, O. (2011): Geomechanical model of the Marmara Sea region - II. 3-D contemporary background stress field, Geophys. J. Int., doi:10.1111/j.1365-1246X.2011.04992.x, 01090-01102.

Hergert, T., Heidbach, O., Bécel, A. & Laigle, M. (2011): Geomechanical model of the Marmara Sea region - I. 3D contemporary kinematics, Geophys. J. Int., 185, doi:10.1111/j.1365-1246X.2011.04991.x, 01073-04189.

Jáky, J. (1944): The coefficient of earth pressure at rest. Journal for Society of Hungarian architects and engineers, 355-358, Budapest, Hungary.

Jaeger, J. C., Cook, N. G. W. & Zimmermann, R. W. (2007): Fundamentals of Rock Mechanics, 4th ed., Blackwell Publishing, Oxford.

Klee, G. (2012): Geothermal borehole Schlattingen 1 - Hydraulic fracturing stress measurements. Nagra Project Report. NPB 12-08. Nagra, Wettingen.

Matter, A., Peters, T., Bläsi, H.R., Meyer, J., Ischi, H. & Meyer, C. (1988): Sondierbohrung Weiach Geologie: Textband. Nagra Technischer Bericht. NTB 86-01. Nagra, Baden.

Mayne, P.W. & Kulhawy, F.H. (1982): K0-OCR relationships in soil. ASCE Journal of Geotechnical Engineering Division 108 (GT6), 851-872.

McGarr, A. & Gay, N. C. (1978): State of Stress in the Earth's Crust, Ann. Rev. Earth Planet. Sci., 6, 405-436.

Nagra (2001): Sondierbohrung Benken – Untersuchungsbericht. Textband und Beilagenband. NAGRA Tech. Bericht NTB 00-01, pp. 328, Wettingen.

Nagra (2002): Geologische Entwicklung der Nordschweiz, Neotektonik und Langzeitszenarien, Zürcher Weinland, NAGRA Techn. Ber. 99-08, pp. 226, Wettingen.

Nagra (2008): Vorschlag geologischer Standortgebiete für ein SMA- und ein HAA-Lager: Geologische Grundlagen (Bericht zur Geologie). Text. NAGRA Technischer Bericht NTB 08-04, pp. 447, Wettingen.

Nagra (2010): Beurteilung der geologischen Unterlagen für die provisorischen Sicherheitsanalysen in SGT Etappe 2. Klärung der Notwendigkeit ergänzender geologischer Untersuchungen, NAGRA Tech. Ber. NTB 10-01, pp. 225, Wettingen.

Richardson, R. M. (1992): Ridge Forces, Absolute Plate Motions, and the Intraplate Stress Field, J. Geophys. Res., 97, 11739-11748.

Simpson, R. W. (1997): Quantifying Anderson's fault types, J. Geophys. Res., 102, 17909-17919.

Zang, A. & Stephansson, O. (2010): Stress in the Earth's Crust, 1st ed., 323 pp., Springer, Heidelberg.

Zoback, M. D. (2010): Reservoir Geomechanics, 2nd edition ed., 449 pp., Cambridge, Cambridge.

Zoback, M. L. (1992): First and second order patterns of stress in the lithosphere: The World Stress Map Project, J. Geophys. Res., 97, 11703-11728.

Zoback, M. L., et al. (1989): Global patterns of tectonic stress, Nature, 341, 291-298.

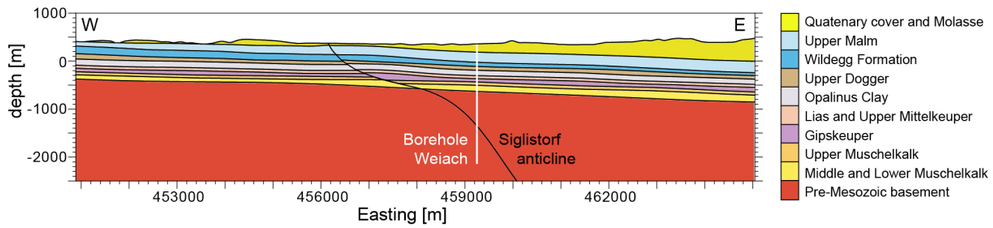

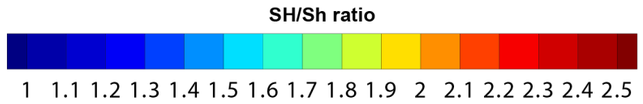

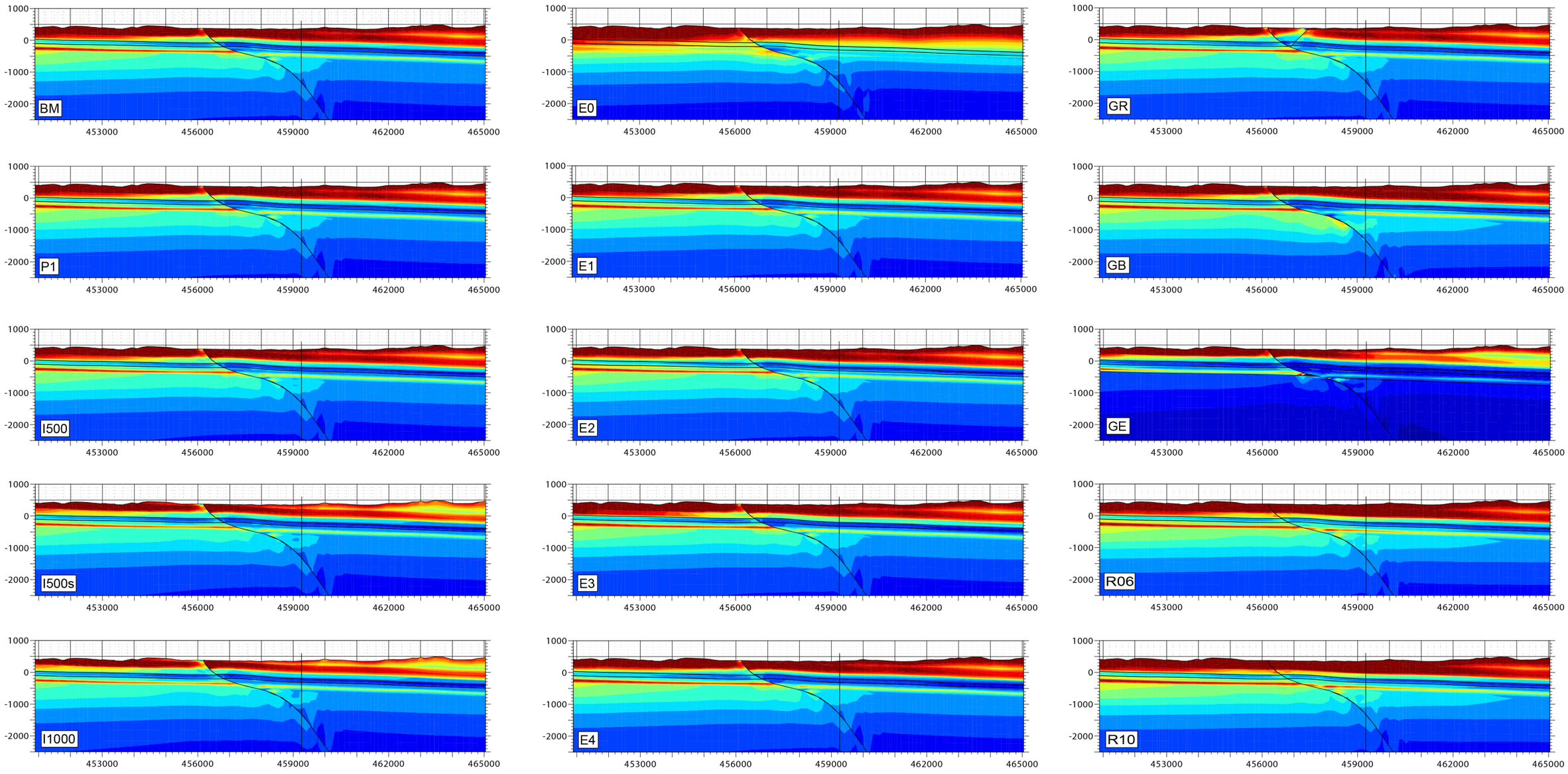

nagra	NAB 13-88
SH/Sh ratio on E-W profiles through Weiach	
	DAT.: Aug. 2014 — **Appendix A-1**

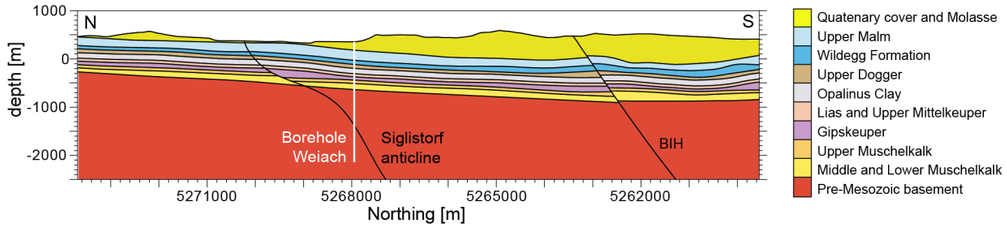

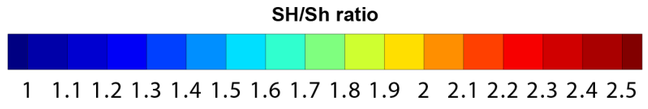

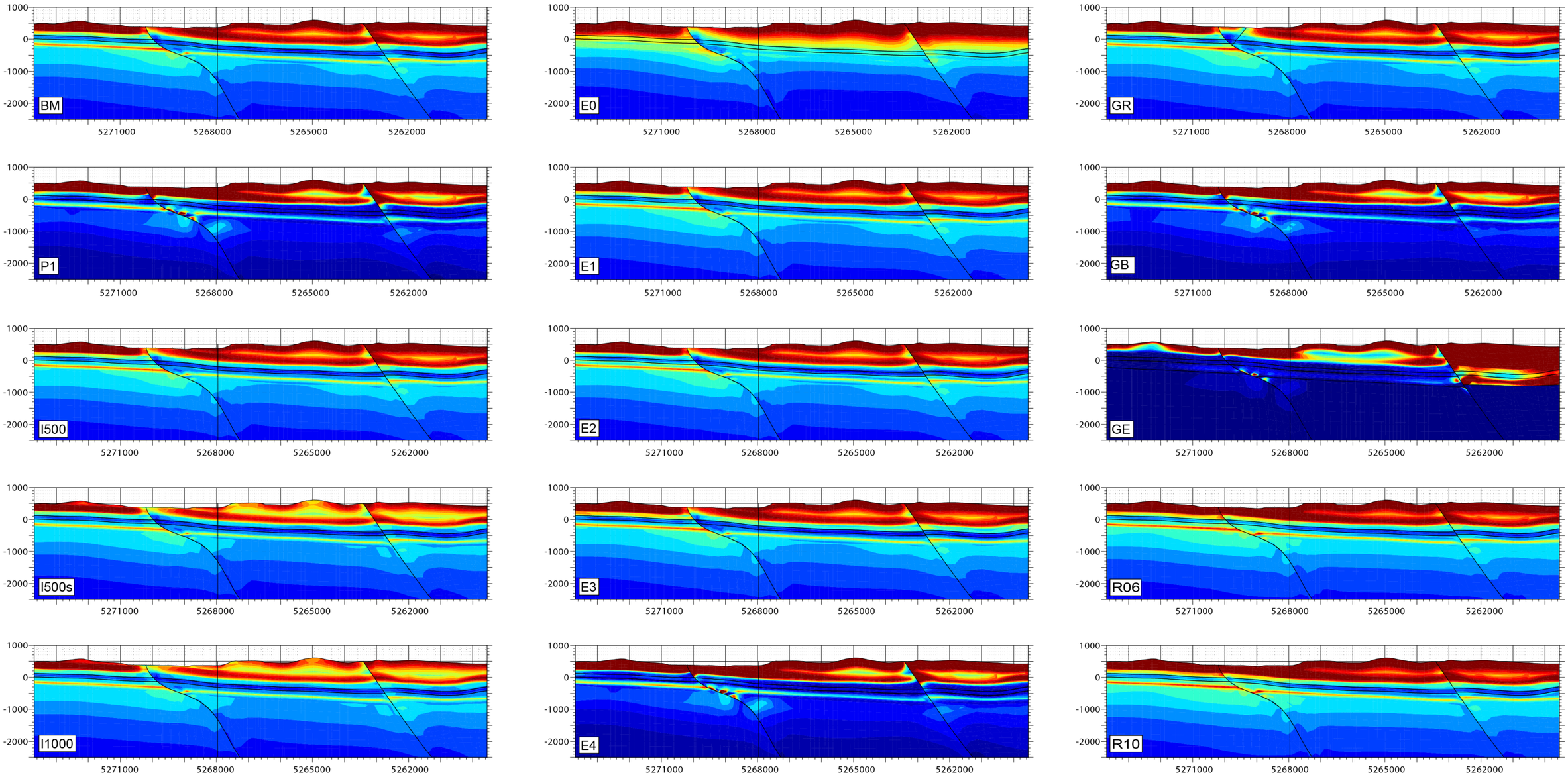

nagra	NAB 13-88
SH/Sh ratio on N-S profiles through Weiach	
	DAT.: Aug. 2014 — **Appendix A-2**

SH/Sh ratio

1 1.05 1.1 1.15 1.2 1.25 1.3 1.35 1.4 1.45 1.5 1.55 1.6 1.65 1.7 1.75 1.8 1.85 1.9 1.95 2

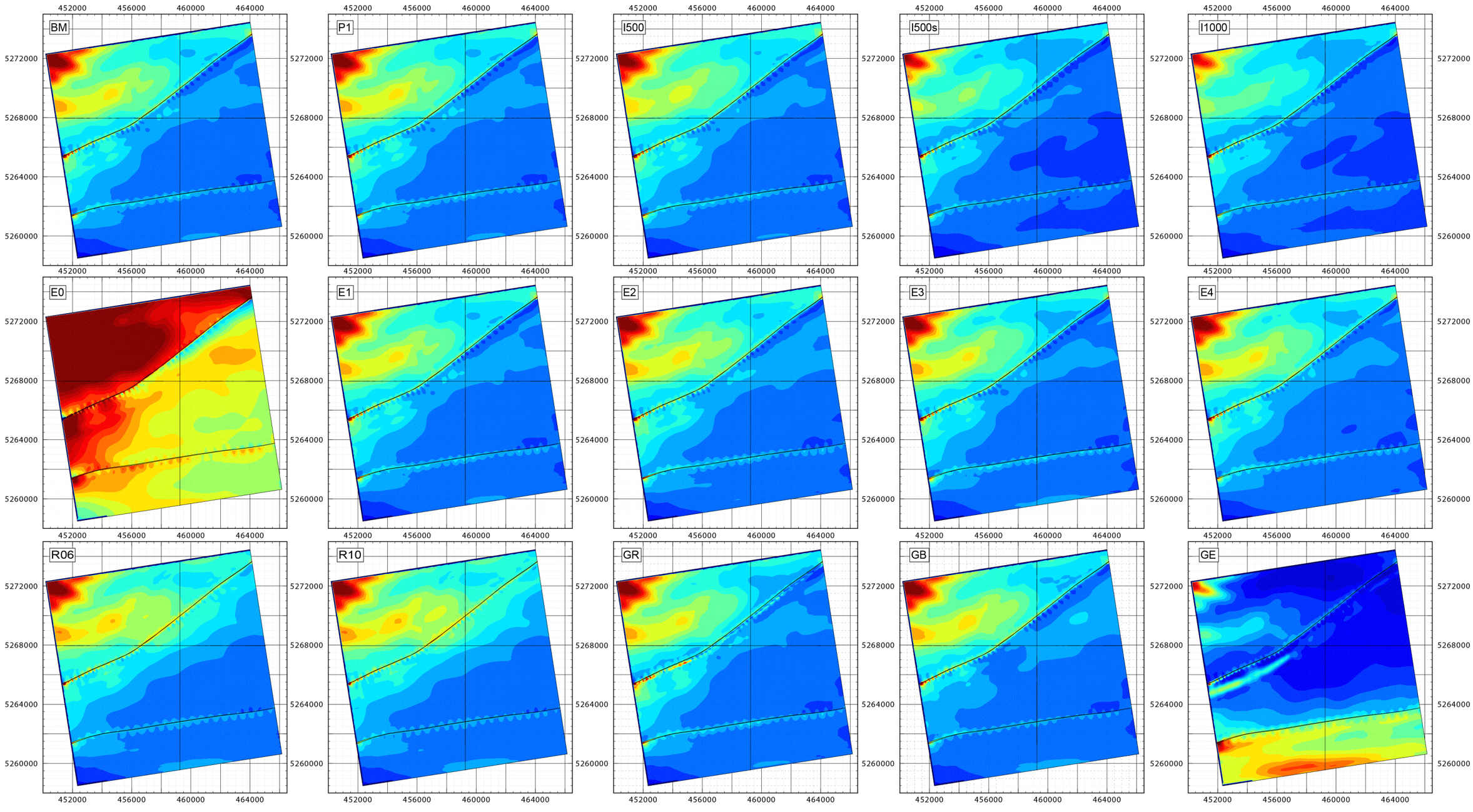

nagra	NAB 13-88
SH/Sh ratio at mean depth of the Opalinus Clay	
	DAT.: Aug. 2014 — **Appendix A-3**

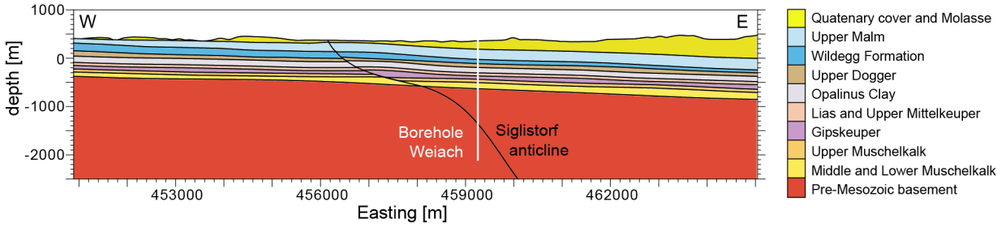

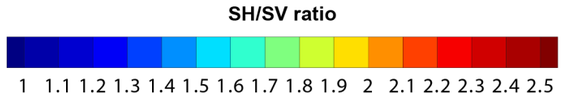

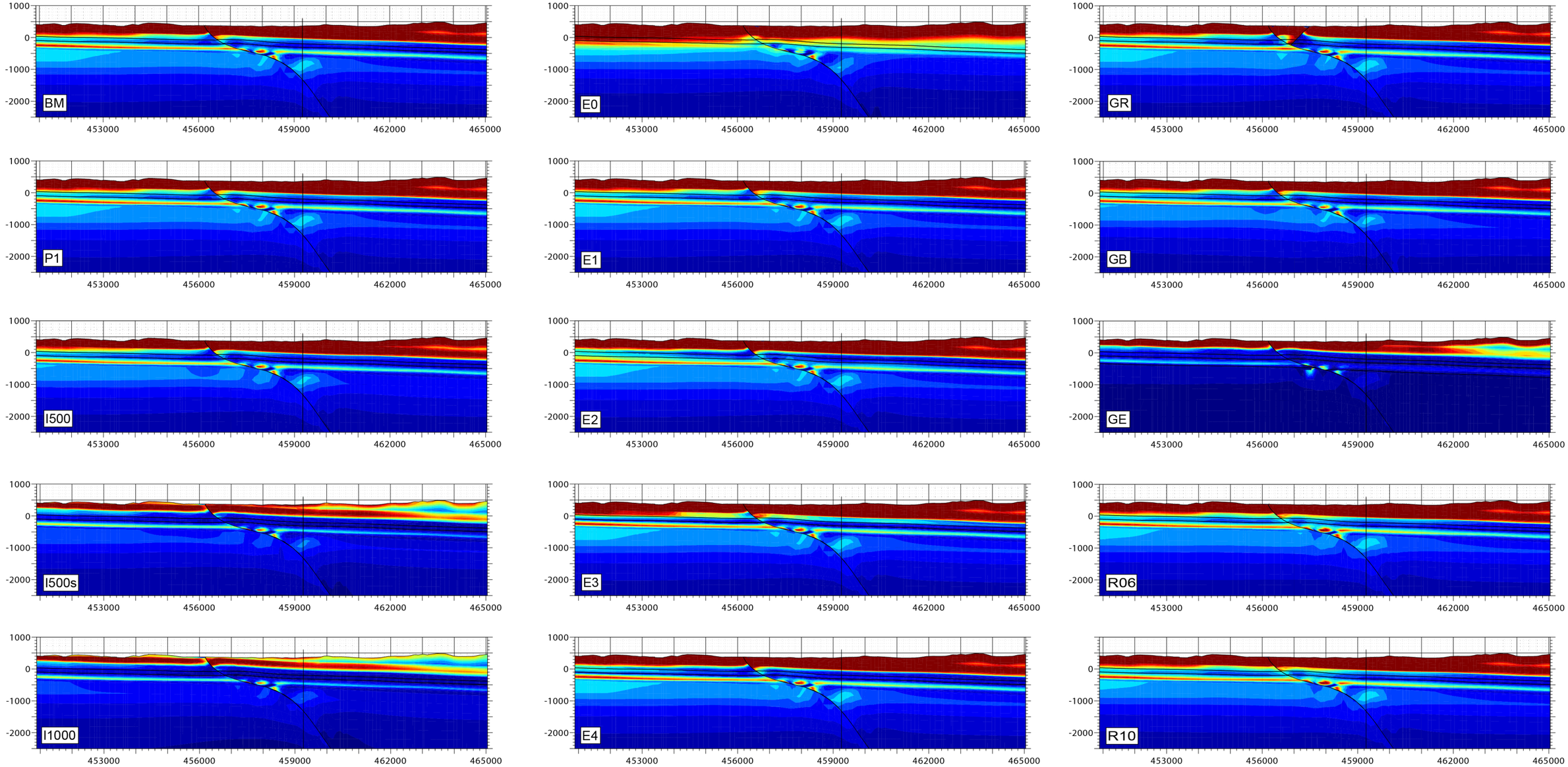

nagra	NAB 13-88
SH/SV ratio on E-W profiles through Weiach	
	DAT.: Aug. 2014 — **Appendix B-1**

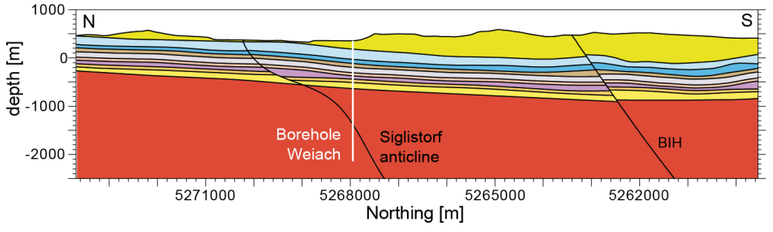

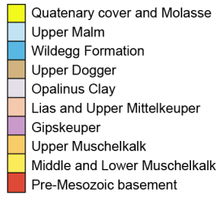

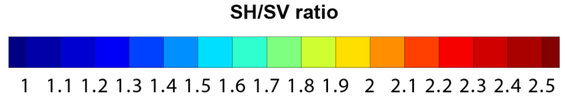

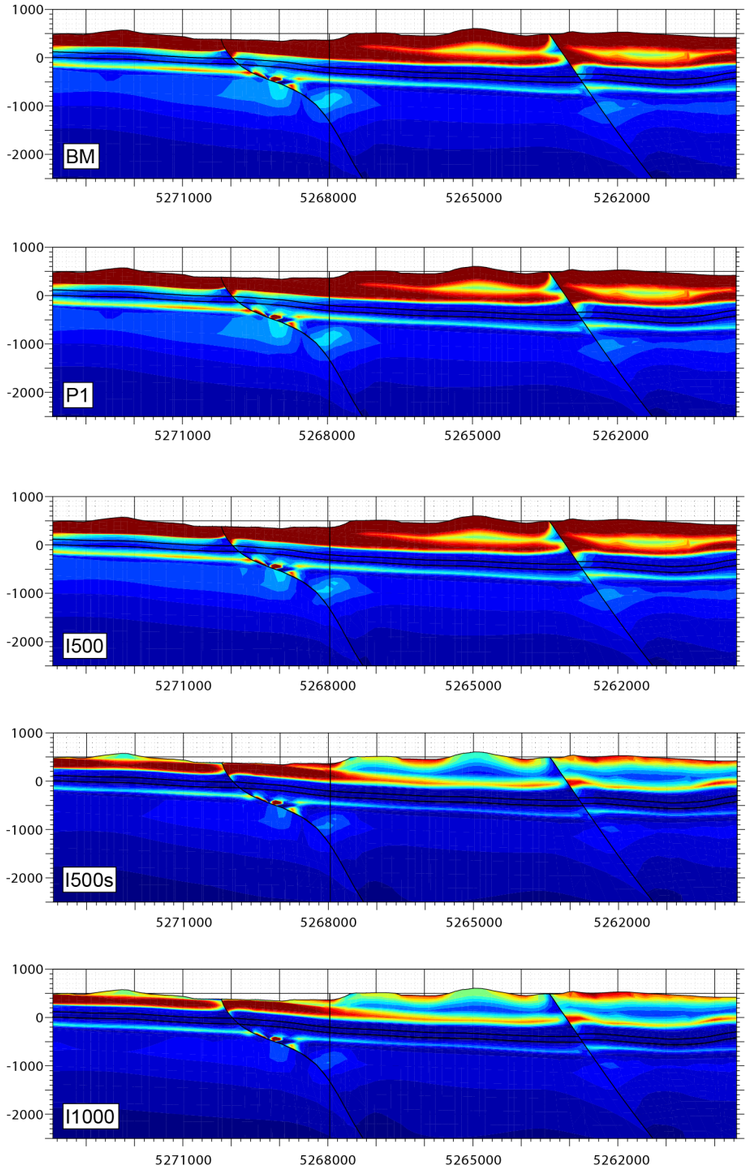

nagra	NAB 13-88
SH/SV ratio on N-S profiles through Weiach	
DAT.: Aug. 2014	**Appendix B-2**

SH/SV ratio

0.8 0.9 1 1.1 1.2 1.3 1.4 1.5 1.6 1.7 1.8

BM P1 I500 I500s I1000

E0 E1 E2 E3 E4

R06 R10 GR GB GE

452000 456000 460000 464000

5272000 5268000 5264000 5260000

nagra	NAB 13-88
SH/SV ratio at mean depth of the Opalinus Clay	
DAT.: Aug. 2014	Appendix B-3

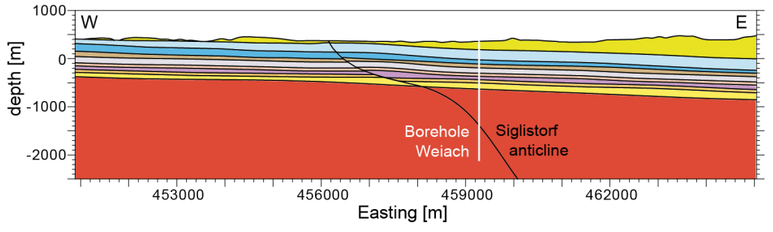

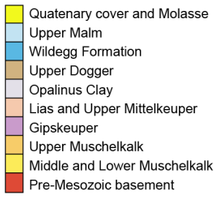

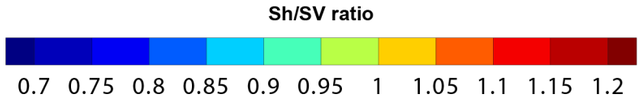

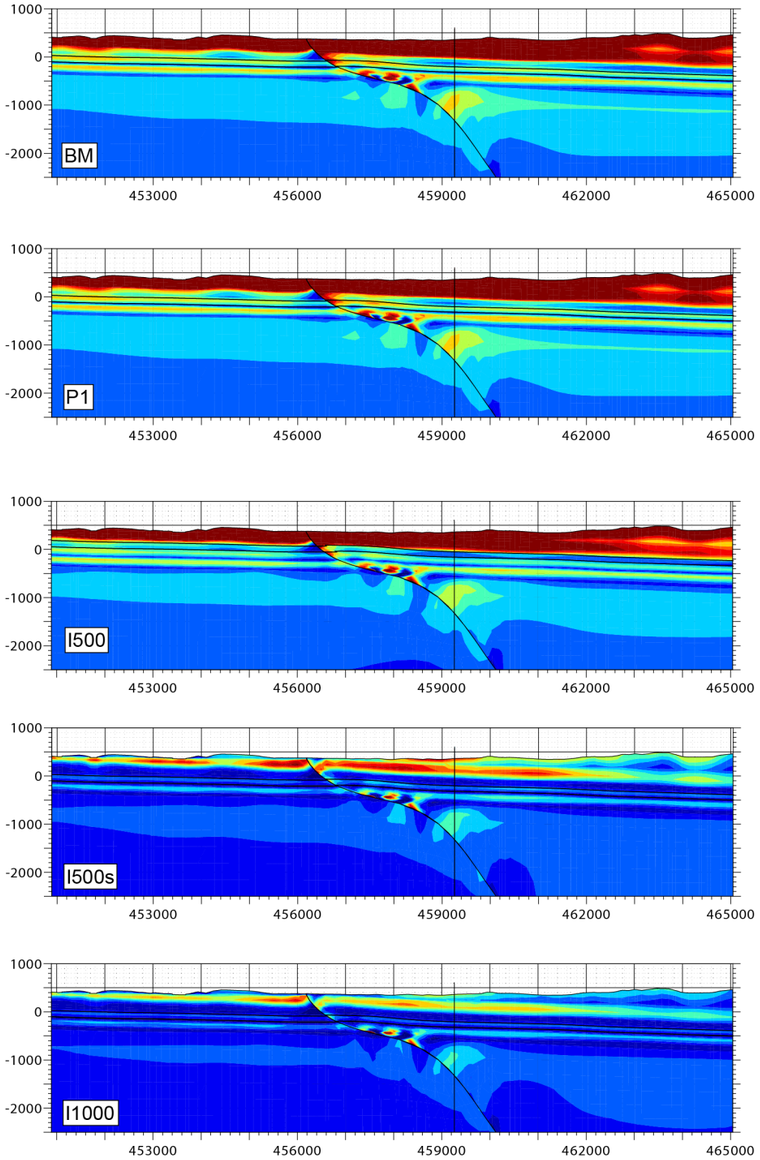

nagra	NAB 13-88
Sh/SV ratio on E-W profiles through Weiach	
DAT.: Aug. 2014	**Appendix C-1**

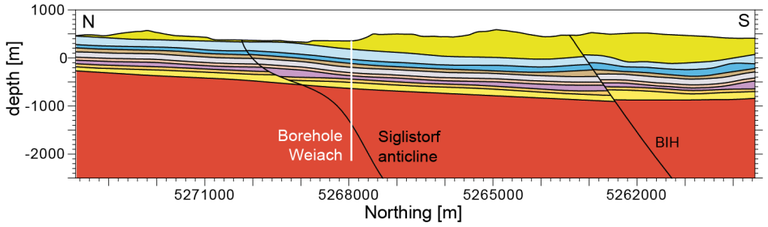

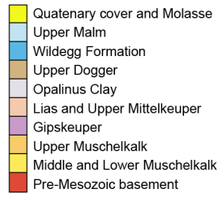

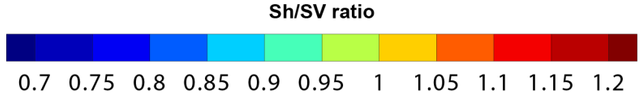

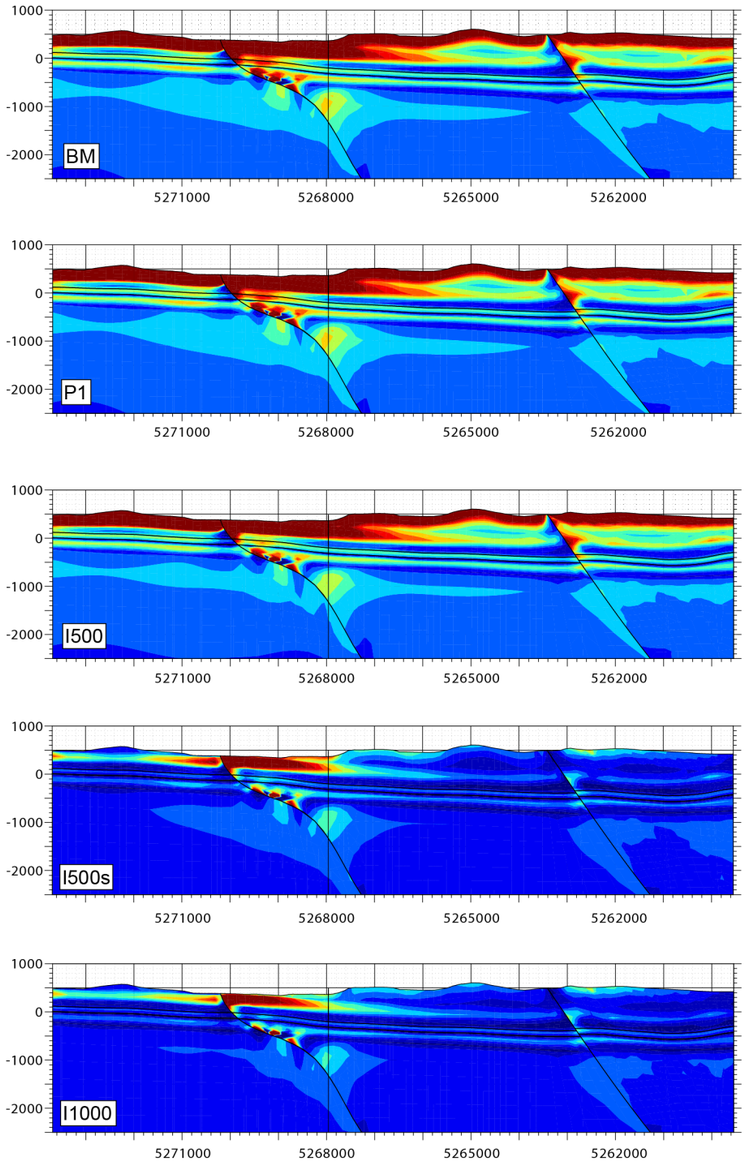

nagra	NAB 13-88
Sh/SV ratio on N-S profiles through Weiach	
DAT.: Aug. 2014	**Appendix C-2**

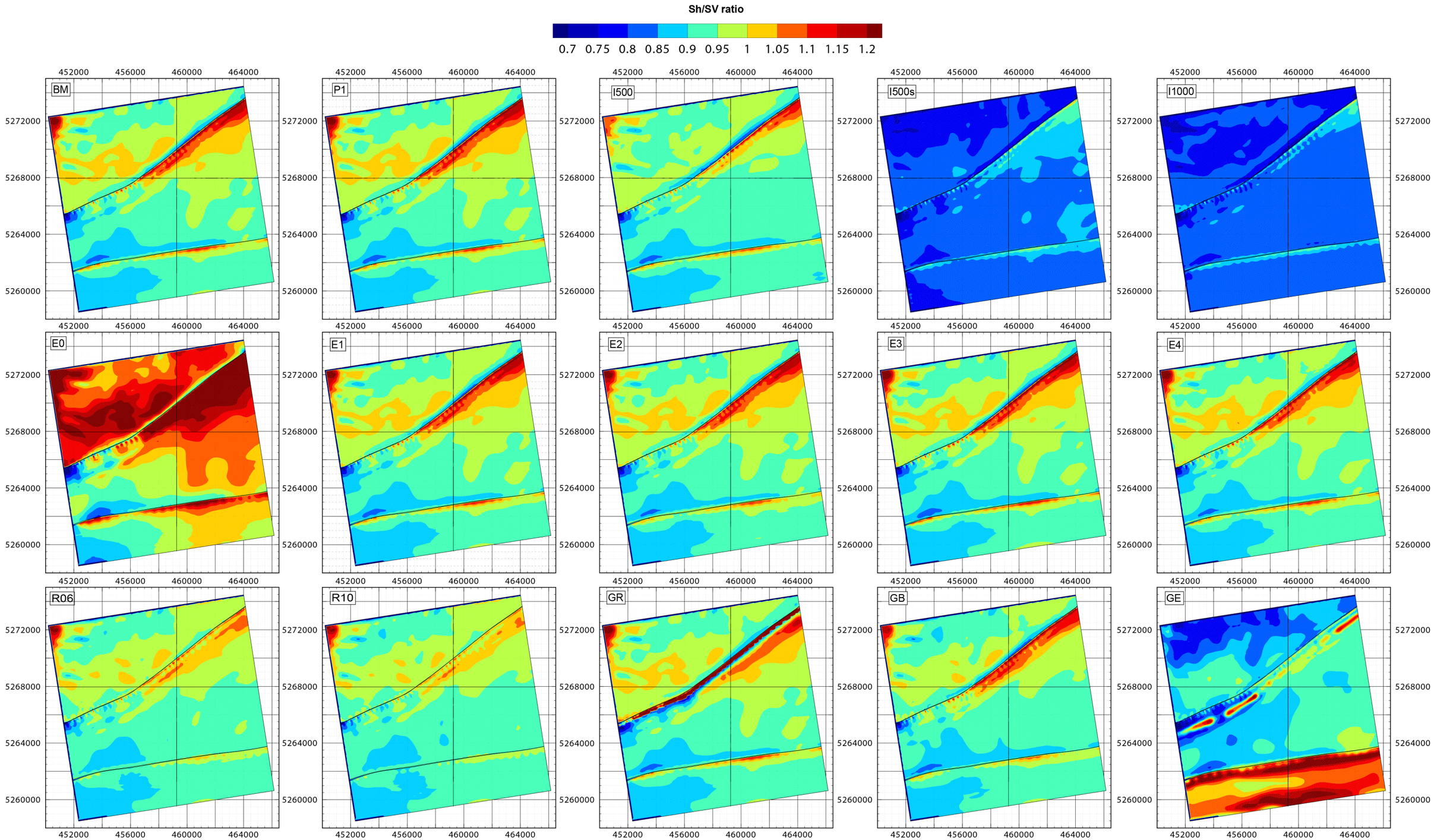

nagra	NAB 13-88
Sh/SV ratio at mean depth of the Opalinus Clay	
DAT.: Aug. 2014	**Appendix C-3**

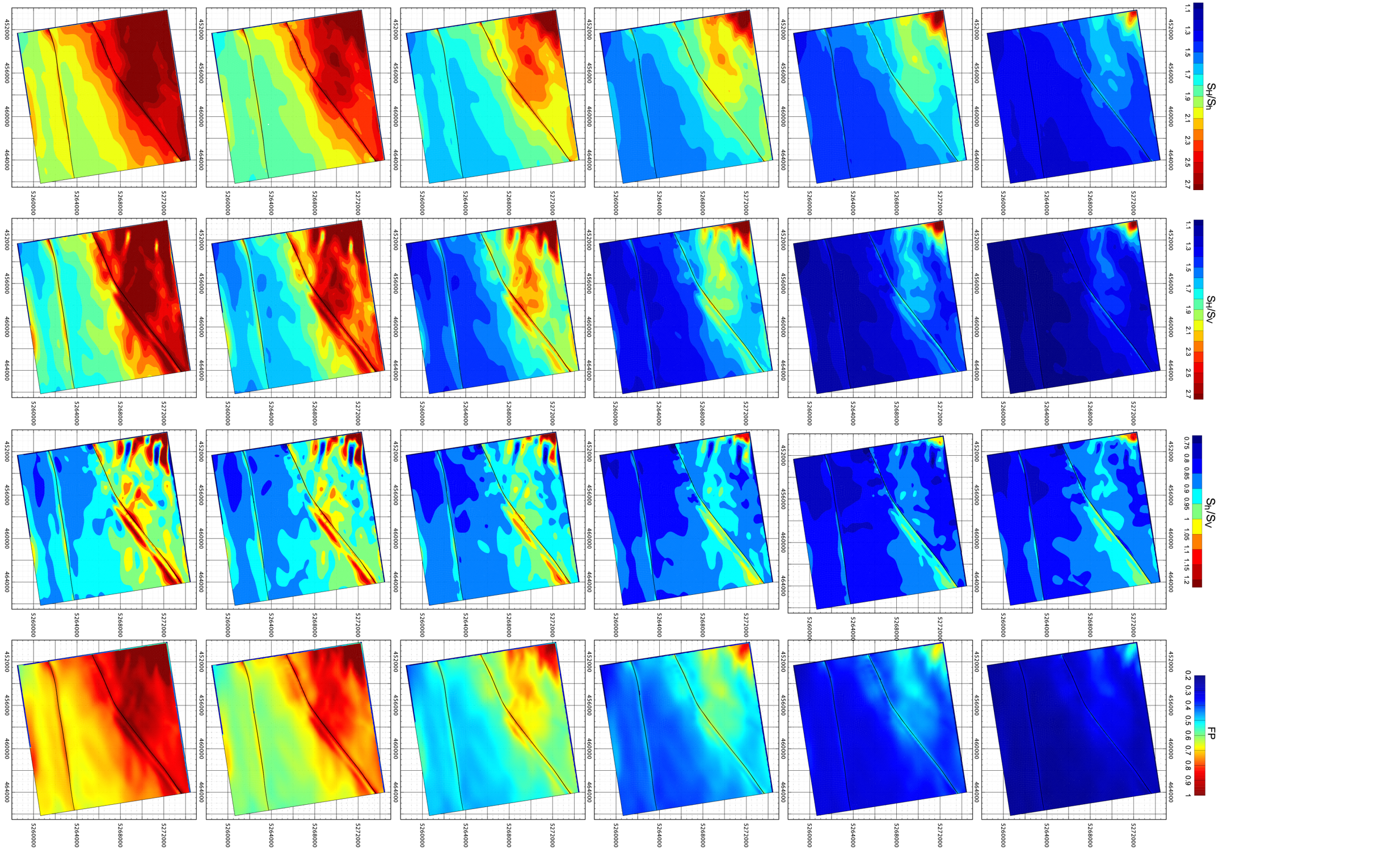

nagra	NAB 13-88
Model P2: Stress ratios and fracture potential (FP) at mean depth of the Opalinus Clay with progressive further NS shortening	
	DAT.: Aug. 2014 **Appendix D**